



Published in final edited form as:

Annu Rev Mater Res. 2011 August 1; 41: 99–132. doi:10.1146/annurev-matsci-062910-100429.

Mussel-Inspired Adhesives and Coatings

Bruce P. Lee¹, P.B. Messersmith^{2,3}, J.N. Israelachvili⁴, and J.H. Waite⁵

¹Department of Biomedical Engineering, Michigan Technological University, Houghton, Michigan 49931; bpl4@yahoo.com

²Nerites Corporation, Madison, Wisconsin 53719

³Department of Biomedical Engineering, Northwestern University, Evanston, Illinois 60201; philm@northwestern.edu

⁴Department of Chemical Engineering, University of California, Santa Barbara, California 93106; jacob@engineering.ucsb.edu

⁵Molecular, Cell & Developmental Biology, University of California, Santa Barbara, California 93106; waite@lifesci.ucsb.edu

Abstract

Mussels attach to solid surfaces in the sea. Their adhesion must be rapid, strong, and tough, or else they will be dislodged and dashed to pieces by the next incoming wave. Given the dearth of synthetic adhesives for wet polar surfaces, much effort has been directed to characterizing and mimicking essential features of the adhesive chemistry practiced by mussels. Studies of these organisms have uncovered important adaptive strategies that help to circumvent the high dielectric and solvation properties of water that typically frustrate adhesion. In a chemical vein, the adhesive proteins of mussels are heavily decorated with Dopa, a catecholic functionality. Various synthetic polymers have been functionalized with catechols to provide diverse adhesive, sealant, coating, and anchoring properties, particularly for critical biomedical applications.

Keywords

adhesion energy; byssus; Dopa; mussel foot proteins; wet adhesion

1. INTRODUCTION

The holdfast of marine mussels has recently provided important chemical and physical insights into moisture-resistant adhesion. This review develops three interconnected themes: how water undermines polymer adhesion, how mussel adhesives and coatings work, and how basic research in this area has translated into diverse applications.

Copyright © 2011 by Annual Reviews. All rights reserved

DISCLOSURE STATEMENT J.N. Israelachvili and J.H. Waite are not aware of any affiliations, memberships, funding, or financial holdings that might be perceived as affecting the objectivity of this review. B.P. Lee and P.B. Messersmith are affiliated with Nerites Corporation, a company that specializes in developing medical adhesives that are synthetic adhesives of mussel adhesive proteins. B.P. Lee is an employee of Nerites, and P.B. Messersmith is a cofounder, director, and consultant of Nerites. Nerites has in the past funded basic research in P.B. Messersmith's laboratory at Northwestern.

2. WATER AND ADHESION

In the technology of adhesive bonding, water or moisture has traditionally been treated as a surface contaminant or weak boundary layer. With few exceptions, the presence of moisture leads to the deterioration of performance in synthetic adhesive polymers. The mechanisms of deterioration are many and complex and include moisture-induced plasticization, swelling, erosion, and hydrolysis of polymers and interfacial wicking and crazing (1).

In biology, water is the medium: Cells and most tissues are approximately 70% water by weight. Saline fluids such as blood plasma, lymph, and seawater surround and bathe cells, tissues, organisms, and implants. The medium has played a crucial role in the evolution of biomolecular adhesion. Water, particularly saline water, limits what can bind and where. At a simplistic molecular level, Coulomb's law for electrostatic interactions predicts that the interaction energy for two point charges $Q_a Q_b$ is $-Q_a Q_b / 4\pi\epsilon r$, where ϵ is the dielectric constant and r is the interionic distance. An electrostatic interaction between opposite charges will be only 1/80 as strong in water ($\epsilon = 80$) as it is under vacuum ($\epsilon = 1$). Actually, the interaction is often further diminished because r will also be increased due to strong solvation of ions such as Mg^{2+} and Li^+ by H_2O (2).

The interaction energies of several other noncovalent interactions such as freely rotating dipole-dipole interactions and dispersion forces are penalized to an even greater degree by the dielectric constant in that $E \propto 1/\epsilon^2$ (2). In contrast, the effect of ϵ on hydrogen bonds is essentially unpredictable; coordination complexes are largely unaffected as long as the ligands of choice bind the metal more strongly than to H_2O (3), and hydrophobic interactions are enhanced by H_2O (2).

Although a molecular perspective is suggestive about the effect of water on interactions between molecules, it must be enlarged where surfaces are concerned. Expanding the concept of interactions between two surfaces in water requires the use of adhesion energies ($E_A = -2\gamma_i$) or works of adhesion ($W_A = 2\gamma_i$, where γ_i is the interfacial energy), which can be measured for an interface between any two homogeneous materials (4). Much theoretical and experimental effort has been devoted to parsing the contributions of electrostatic, polar, and dispersion forces to interfacial energies. An illustrative example of how water affects adhesion in terms of interfacial energies is a comparison of epoxy on aluminum under clean-room and fully hydrated conditions (Figure 1) (5). The polar and dispersive components of each interfacial energy can be summed to estimate a W_A . This work is quite strong (positive) in vacuum, whereas in water there is no measurable adhesion, e.g., $W_A = -137 \text{ mJ m}^{-2}$. The most subversive component undermining adhesion in the latter case derives from the product of the polar components in the interaction between aluminum and water, i.e., $\gamma_2^p \gamma_w^p$ (-164 mJ m^{-2} in Figure 1), which the polymer interactions with the metal are unable to overcome. This example shows that successful adhesives for wet polar surfaces must be designed so as to result in a more favorable interaction with a target polar surface than water is able to offer. Engineering covalent bonds into the interfaces of moisture-resistant adhesives is currently quite common but requires elaborate and costly clean-room procedures (5). Understanding mussel adhesion offers insights into how this can be done entirely underwater.

3. BYSSUS: THE MUSSEL HOLDFAST

Rocky wave- and windswept seacoasts are havens for mussels (particularly those in the genus *Mytilus*)—wedge-shaped bivalve mollusks that blanket the rocks of the intertidal zone (6, 7). The rocky seaside habitat offers mussels many attractive benefits such as aerated seawater for respiratory gas exchange, rapid waste removal, rich nutrient supply, and the

security of a highly interactive community (8). The habitat also exacts costs, including the holdfast termed the byssus (Figure 2a). Making and maintaining a byssus are absolutely necessary adaptations to resist the lift and drag of waves in the intertidal zone and cost between 8% and 12% of the total metabolic energy of a mussel (9, 10).

3.1. Organization and Fabrication

The byssus is essentially a bundle of radially distributed threads and consists of four parts: attachment plaques, threads (distal and proximal portions), stem, and root. The expanded plaques at the distal thread ends are attached to foreign surfaces, whereas the proximal ends radiate from the stem, which merges with the living tissues of the mussel by way of the root (Figure 2b). The relationship of a mussel to its byssus is a peculiar one akin perhaps to a futuristic bionic device: Retractor muscles within the mussel (living) dovetail with fibrous byssal proteins (nonliving) in the root, the interface between living and nonliving tissues. Like silkworm silk, byssal threads are rapidly made of protein and are void of living cells, but unlike silk, they remain attached to the root at the base of the mussel foot, where an assortment of 12 retractor muscles controls thread tension.

The foot makes byssal threads one at a time in a process that resembles reaction injection molding and requires approximately 3–10 min per thread (11). Accordingly, the mussel's tongue-like foot emerges from the ventral shell gap and explores available surfaces within a radius of approximately 5–6 cm. Besides the discoveries that the mussel prefers high-energy surfaces to low-energy surfaces and rough surfaces to smooth surfaces, investigations of the mussel's sensory powers of surface discrimination have been limited (12, 13). Upon finding a suitable spot, the foot tip attaches to the surface and becomes quite motionless.

3.2. Tenacity

The average mussel has 50 to 100 threads at any given time, and these threads are roughly radially arranged over a flat surface. Field tests of mussel tenacity or the resistance to dislodgement have been measured with handheld force gauges in normal and parallel displacement modes. Adjusted for mass, the tenacity of a solitary (length 10 cm and weight ~0.150 kg) California mussel (*Mytilus californianus*) attached to a rock is typically approximately 300 N in normal mode (lift) and 180 N in parallel displacement mode (drag) (Figure 3) (14, 15). Tenacities in other *Mytilus* species are less than half these figures. As all threads contribute to load bearing only in normal mode, 300 N divided by 50 threads yields 6 N per thread. The geometry of load transfer in byssus during normal and parallel extension has been examined in greater detail elsewhere (14, 15). The most common point of failure in tenacity tests is the adhesive plaque. If one takes 2 mm as the diameter of each plaque, an estimate for average plaque adhesive strength in a solitary field mussel is 6 MPa. This value is considerably higher than the 0.3 MPa measured directly on individual plaques by Allen et al. (16) and Wilker and colleagues (17) in *Mytilus edulis*. Perhaps the disparity reflects a species dependency, but a significant concern about these measurements is that the angle of contact between a thread and a plaque decreases as the distance between the plaque and the thread origin increases. More importantly, the point of contact between a distant plaque and its connecting thread is shifted to the proximal edge of the plaque (Figure 3). Mature mussels have threads that can exceed 5–6 cm, making the angle between the thread, plaque, and substratum very small. As Lin et al. (18) point out, applying a normal force to a thread with a 5° plaque contact angle is likely to fail in peeling at a much lower force than for a thread with a natural 90° angle to the plaque. Unfortunately, even today researchers determine plaque attachment strengths without taking note of the thread-plaque contact angles (17). At any rate, if one sets aside the concern of angles, even a 6-MPa attachment strength in plaques is not particularly impressive for a high-performance adhesive.

Nonetheless, the observed adhesion is a remarkable achievement given the ever-present seawater and the fouled surfaces that mussels must contend with.

3.3. Byssal Plaques

All portions of the mussel byssus are critical for secure attachment. Byssal plaques, however, are specialized for adhesion to solid foreign surfaces.

3.3.1. Microstructure—Mussel byssal plaques have a surprising degree of fine and hierarchical structure (Figure 4*a–c*). Although there is much old literature on the subject, we confine ourselves to transmission electron microscopy (TEM) and freeze-fracture analyses (19). The distal thread core consists of bundles of microfibrils separated by a granular matrix. As each thread approaches the plaque, the bundles splay out like tree roots into the porous bulk of the plaque, approaching to within 1 μm of the interface (Figure 4*c*). The plaque exhibits an ~40% porosity and a marked gradient in pore diameter: The diameter is only 200 nm near the substratum but nearly 3 μm where the thread meets the plaque. The pores are open, are interconnected by channels with smooth walls (Figure 4*d*), and are filled with fluid in their native state. The trabeculae also consist of an open-pore network in which pores range in diameter from 50 to 500 nm and walls are only 50 nm thick.

With respect to the interface, plaques attached to glass prepared for examination by SEM appear mostly delaminated, but closer scrutiny of the interfacial region reveals fibrous foci or pillars that remain intact (Figure 4*e*). These pillars suggest that strong adhesive contacts between the plaque proteins and marine surfaces are possible in plaques. The limiting factor for mussel adhesion may thus be the extent to which surfaces are fouled by other contaminants (e.g., conditioning layers and biofilms) (20). As biofilms are rarely, if ever, uniform on marine surfaces, mussel adhesion may be determined by whether adhesive proteins in the plaque find strong footholds in the occasional bare patches of solid surface.

3.3.2. Protein biochemistry—*Mytilus* byssus contains roughly 25–30 different proteins. Perhaps 7–8 of these are present in the plaque, but only 5 are unique to plaque. Plaque proteins not confined to the plaque are mussel foot protein (mfp)-1, prepolymerized collagens (preCOLs) preCOL-D and preCOL-NG, and thread matrix proteins (i.e., tmp-1). Mfp-1 is the key protein of the byssal cuticle and is discussed in Section 3.4. The other proteins that assemble to make up the thread are discussed elsewhere (21). Those proteins confined to plaques are mfp-2, -3, -4, -5, and -6 (Table 1). All these proteins contain the posttranslationally modified amino acid 3,4-dihydroxyphenyl-L-alanine (Dopa) and have high isoelectric points but otherwise have widely different sequences. Most are polymorphic families—there are multiple genes and gene copies—or are processed via alternative splicing.

3.3.2.1. Mfp-2: Mfp-2 is the most abundant plaque protein, representing 25 wt% of the plaque. It is 45 kDa long and consists of 11 tandem repeats of an epidermal growth factor (EGF) domain that resembles a knot stabilized by three disulfide bonds and is a common motif in extracellular matrix proteins (22). Dopa (<5 mol%) is clustered at the N and C termini and otherwise appears once or twice on each EGF repeat. Rzepecki et al. (23) detected at least eight mfp-2 sequence variants in *M. edulis* plaques. One complete complementary DNA (cDNA)-deduced protein sequence has been published, but several others are accessible in the UniProt (ExPASy) database. At least one of the EGF repeats has a consensus motif for Ca^{2+} binding (24).

3.3.2.2. Mfp-3: Mfp-3 is the most polymorphic of all plaque proteins. Perhaps as many as 35 different sequence variants exist, although not all are necessarily expressed in each

plaque (25). Moreover, there is extensive variation due to posttranslational modification of protein tyrosine and arginine to Dopa and 4-hydroxyarginine, respectively. Such variation is immediately evident in purified variants by the number of peaks separated by 16 Da, as detected by mass spectrometry (26, 27). Protein masses for the entire family range between 5 and 7.5 kDa (27). Electrophoretically, the variants cluster into two groups known as slow- and fast-moving isoforms. The latter are Dopa rich, with typically 20 mol% or more and with high positive-charge density; the former, in contrast, have lower Dopa (5–10 mol%) and lower charge density (27). Only a few other amino acids—glycine, asparagine, tryptophan, and lysine—are typically represented at higher than 10 mol% in mfp-3 and are immediately evident in the chemical structure of mfp-3 variant f (Figure 5). In plaque footprint analyses using in situ MALDI-TOF (matrix-assisted laser desorption ionization time of flight) mass spectrometry, mfp-3s are always abundantly evident.

3.3.2.2. Mfp-4: Mfp-4 is one of the larger plaque proteins at 90 kDa and has been fully sequenced only from *M. californianus*. It contains a peculiar histidine-rich decapeptide repeated 35 times in tandem and binds copper with high capacity (28). Dopa levels are low and are confined to the protein's N and C termini. Dopa is the only modification identified to date. Because mfp-4 has a distribution biased toward the proximal end of the plaque, it was proposed to interact with the histidine-rich ends of preCOLs via copper complexes (28), but this remains to be confirmed in situ.

3.3.2.4. Mfp-5: Mfp-5 is the least polymorphic of the plaque proteins: A single sequence was detected in *M. edulis*, and *M. californianus* plaques contain two closely related variants (29, 30). The protein has 99 residues, of which 28 are consistently Dopa. Serine is also variably modified to phosphoserine (Table 1). The other abundant residues are glycine and lysine. Mfp-5 has the highest charge density, i.e., one per three residues, of all plaque proteins. In plaque footprint analyses using in situ MALDI-TOF mass spectrometry, mfp-5 is usually present but in sparing amounts and requires very high laser power. Desorption and ionization of a footprint protein from a surface during MALDI are good evidence of its presence. Lack of a signal, however, is not compelling evidence of its absence. As is the case with mfp-5, strong adsorption to a surface can limit desorption during MALDI.

3.3.2.5. Mfp-6: Like other footprint proteins, e.g., mfp-5, mfp-6 contains high levels of lysine, tyrosine, and glycine, but Dopa content is typically less than 2 mol% (30). Moreover, cysteine is at 11 mol%, of which only a small proportion occurs as the disulfide cysteine. The high thiol content at first suggested that mfp-6 may use cysteines as nucleophiles of Dopaquinones to form cysteinyl-Dopa cross-links—a stable way to couple to other proteins in the plaque (30). Although 5-*S*-cysteinyl-Dopa is detectable in the plaque of *M. californianus* at ~1 mol%, this is not the only role of mfp-6, which is also critical in maintaining the redox balance during footprint formation. Mfp-6 effectively reduces Dopaquinones back to Dopa, coupling this half-reaction to the oxidation of two thiols to a disulfide (31).

3.3.2.6. PreCOLs: PreCOL represents a family of block copolymer-like natural fusion proteins that self-assemble to form the fibrous core of byssal threads. There are three major types of pre-COLs: preCOL-D, preCOL-P, and preCOL-NG. The distinguishing letters reflect distribution trends within the thread, i.e., distal (D), proximal (P), and nongraded (NG) (32–34). The collagen block or domain is in the center and is characterized as in other collagens by [glycine-AA₂-AA₃]_n repeats (where AA denotes amino acid) representing a little less than half the total mass of each chain in the preCOL trimer. Flanking either side of the collagen domain are theme domains that help define the thread's local stiffness. In preCOL-D, flanking domains are distinctly spidroin like, whereas in preCOL-P, the flanking domain sequence resembles the pentapeptide repeats of elastin X-Gly-X-Pro-Gly, where Gly

denotes glycine, X denotes another glycine or a nonpolar amino acid, and Pro denotes proline. N- and C-terminal domains of the preCOLs are histidine rich (≥ 20 mol%). Mussels mold the preCOLs as liquid crystals separated by glycine- and asparagine-rich matrix proteins (Table 1) (35) into thread-like shapes in the ventral groove of the foot (11). Cooperative metal binding by the terminal histidines is believed to lock the preCOL assembly into cohesive fibers (34) and may mediate interactions between preCOLs and mfp-4 (28). PreCOLs are crucial for the tenacity of byssal threads but probably do not participate in plaque adhesion to surfaces. The splayed-out, root-like fibers embedded in the plaque matrix appear to be preCOL-D and preCOL-NG, but plaque-specific collagens are also possible.

3.3.3. Localization—Given the extent of epitope concealment induced by metal-mediated and covalent protein cross-linking, traditional histochemical and immunohistochemical techniques have not been able to deconstruct with any certainty much of the chemistry of byssal plaques (36, 37). Innovative alternative approaches, however, are yielding deeper insights. Plaque footprints, i.e., the lower interfacial $1\ \mu\text{m}$ or so, are conducive to interrogation by MALDI-TOF mass spectrometry. With sinapinic or α -cyano 3-hydroxycinnamic acid as the matrix, mfp-3s are detectable at most laser energies, whereas mfp-5 and mfp-6 require significantly higher energies for detection at the same intensity (27, 30). Above the interface and deeper within the plaque core, MALDI loses its charm, but useful information can be gleaned using Raman microscopy by following the frequencies of functionalities unique to one mfp or another. For example, the strong resonance Raman signals associated with the byssal cuticle (38) are identical to those of purified mfp-1 and Fe^{3+} (39). Additional but different resonance signals are also apparent in the plaque core, where they are colocalized with the phenylalanines of plaque mfp-2 and perhaps mfp-6 (24). Mfp-4 seems preferentially localized at the nexus between the thread and plaque (28). Electron paramagnetic resonance spectroscopy has also been used to detect Fe^{3+} and semiquinones in plaques (40), but its spatial resolution is low. Figure 6a summarizes the current view of mfp distribution in the plaque.

3.3.4. Molecular interactions—The interactions between specific mfps and between mfps and surfaces in aqueous solutions have been investigated using the surface forces apparatus (SFA), an instrument with angstrom distance and nanonewton force precision (2, 5). The SFA can measure (a) the repulsive or attractive forces during approach; (b) the attractive adhesion forces, if any, upon separating two surfaces in air or solution; and/or (c) the attractive forces between a surface and a liquid underwater (18, 24). The measured forces reflect the nature of interaction between the proteins or between the proteins and a mineral surface such as mica. Separation of two surfaces against an attractive interaction between them in the SFA typically involves breaking protein-protein (cohesive) and protein-surface (adhesive/adsorptive) interactions, which can usually be resolved. Lowering the protein concentration, for example, to a point at which the protein forms a monomolecular film in an asymmetric testing geometry (Table 2, inset) can provide a clearer approximation of the adsorptive component of the attractive forces because primarily covalent bonds within the same protein chain are cohesively stretched (Table 2).

Mfp films that exhibit attractive forces during separation are said to bridge, whereas those that bind one surface but do not cross over to the other are coating-only films, e.g., mfp-1 (18). Mfp-3 and mfp-5 show bridging in both symmetric and asymmetric configurations, at all tested concentrations, and on all surfaces tested (18, 41; E. Danner, M. Hammer, J. Israelachvili & J.H. Waite, unpublished). With the notable exception of mfp-1, the higher the Dopa content, the stronger is the observed bridging adhesion on mica surfaces (Table 2) (41). For example, mfp-5 with 30-mol% Dopa is the best adhesive, with a maximum W_A at $\sim 6\text{mJm}^{-2}$ —nearly three times that of mfp-3 with 20-mol% Dopa. Hydrogen bonding by

Dopa to the mica surface is thought to be bidentate, with both phenolic hydroxyls of Dopa as hydrogen donors to oxygen hydrogen acceptors on the polysiloxane surface of freshly cleaved mica. The two mutually well-oriented double –OH bonds in the Dopa-mica interaction, for example, may give only twice the energy E of a hydrogen bond ($\sim 14kT \times 2$) but 10^6 times the lifetime τ because τ is proportional to $e^{-E/kT}$ (2). This is essentially the same situation and configuration as in the more familiar association of A-T pairs in DNA.

Typically, due to the low solubility of many mfps at $\text{pH} \geq 6$, SFA tests are conducted at pH 5.5. This is not the pH of strongest mfp adhesion to mica; however, at this time 5.5 appears to best approximate the pH of protein secretion by mussels (31). Films of mfp-1, -2, -4, and -6 show little to no intrinsic interaction in both symmetric (film deposited on both mica surfaces) and asymmetric (film on one mica surface only) tests, but adhesion can be extrinsically improved by adding certain metal ions (Table 2).

In asymmetric tests with the two mica surfaces coated by different protein films, the specificity of protein-protein interactions really emerges (Table 2, inset). For example, mfp-2 binds instantaneously to mfp-5 but not to mfp-3 (24). In fact, mfp-3 appears to displace mfp-2 from mica so that eventually the bridging adhesion that develops between the mica surfaces is solely from mfp-3 bridging (31). Mfp-3 and mfp-5 exhibit a very strong interaction—up to 2.5 mJ m^{-2} —significantly more than mfp-3 by itself to mica (J.N. Israelachvili & J.H. Waite, unpublished data). Mfp-2 shows no intrinsic interaction with mfp-1, -4, or -6. The role of Dopa, if any, in the intrinsic interactions between different mfps is not currently understood. Figure 6*b* summarizes known interactions of mfps located near the plaque-substratum interface. Additional factors greatly enhance the versatility of these interactions, as discussed below.

3.3.5. Other interaction factors—Recently, it has been possible to measure the adhesion of mfp-3 in symmetric or asymmetric modes at pH 7.5 (31). Adhesion to mica at higher pH is reduced by $\sim 95\%$ relative to pH 3 and by $\sim 75\%$ relative to pH 5 (Figure 7*a*). This result was expected because Dopa oxidation leads to Dopaquinone formation, which is significantly less sticky than Dopa on many surfaces, including mica and titania (see Section 4). However, the result begs the question as to why a mussel would rely on Dopa proteins for adhesion if they succumbed so easily to oxidation; the pH of seawater is even higher at 8.2. Adhesive proteins such as mfp-3 and -5 do not succumb to oxidation because they are secreted at low pH (pH 5–6) into a confined space, where they are maintained in a reducing environment in the plaque footprint (31). The redox balance in the footprint is controlled by mfp-6, a cysteine-rich protein in which only one to three of the cysteines are detectable as thiols (30, 31), but these cysteines are distinguished by having very low $\text{p}K_a$ s of ~ 3 –5; in contrast, a typical cysteine $\text{p}K_a$ is 8–9. Diminished adhesion in mfp-3, caused by raising the pH from 5.5 to 7.5, can be rescued by the addition of picomoles of mfp-6 to the gap at pH 5.5 (Figure 7*b*). Partial rescue of Dopa is instantaneous, but complete rescue occurs in 60 min. That thiols in mfp-6 are responsible for redox was demonstrated by a loss of Dopa rescue (and adhesion) following *S*-carboxymethylation of mfp-6 as well as by the replacement of mfp-6 with 1,6-hexane dithiol (31, 41).

3.3.5.1. Metal ions: Metal ions, especially di- and trivalent cations, can enable adhesion of non-adhering mfps to a surprising degree. Metal effects are most striking for mfp-2 and mfp-1 (see Section 3.4). As the most abundant plaque protein (at more than 25 wt%), one molecule of mfp-2 has a one-in-four probability of encountering another mfp-2. The inability to interact with this neighbor would undermine cohesion in the plaque. Ca^{2+} improves the W_A between mfp-2s from 0 to nearly 0.4 mJ m^{-2} (24). Fe^{3+} addition increases the adhesion of mfp-2s to 3 mJ m^{-2} (Figure 6*b*), but the effect takes nearly 60 min in the SFA, perhaps because of the slow rearrangement of the bulky EGF domains. At pH 7,

rearrangement is faster, but the strength of adhesion remains unchanged. Fe^{3+} and Ca^{2+} also have measurable effects on the adhesive interactions of the other mfps (24). For example, the presence of $10\text{-}\mu\text{MFe}^{3+}$ diminishes interactions between two symmetric mfp-5 or mfp-3 films (24).

3.3.5.2. Physical factors: The discovery that basic Dopa-containing proteins are mixed with polyanionic proteins (isoelectric point ≈ 2) in sandcastle worm (*Phragmatopoma californica*) cement with more than 40-mol% phosphoserine has suggested that mussel adhesives may also be dispensed as complex coacervates (42–44). Low-isoelectric-point proteins also exist in the byssal plaque but are insufficiently characterized for description here. Complex coacervation is a process in which aqueous solutions of polyanions and polycations undergo phase separation at a pH at which they electrically neutralize each other. The denser, smaller phase is polymer rich, with protein concentrations reaching as high as $1\text{--}2\text{ g cc}^{-1}$. Although it is too early to speculate on the details of how marine organisms practice coacervation, coacervation has considerable potential for wet adhesion, including phase-separated fluidity, reduced viscosity, low interfacial energy, and high internal protein and solvent diffusion coefficients (44). Coacervates made from a cationic recombinant mfp fusion protein and hyaluronic acid (HA) possess properties consistent with predictions (44, 45). At an optimal 1:3 mixing ratio of HA:recombinant mfp, the bicontinuous fluid exhibited an interfacial energy of $<1\text{ mJ m}^{-2}$, shear-thinning viscosity ranging from 100 to 10 Pa·s, and a protein concentration of 0.5 g cc^{-1} —all properties well adapted to underwater adhesion.

3.4. Byssal Coating

The role of coatings in enhancing the performance of underlying materials is increasingly appreciated in manufacturing. Undoubtedly, natural coatings have equally important roles; however, until recently, the coating of mussel byssus was completely overlooked.

3.4.1. Function and mechanical properties—The byssal coating or cuticle is a 2–5- μm -thick layer covering all parts of mussel byssus exposed to seawater (Figure 8a,b). One function attributed to the cuticle is insulation of the fibrous collagenous core against microbial attack (46). This function is quite plausible but has not been directly demonstrated.

However, byssal cuticles also have mechanical properties with obvious adaptive value, as revealed by recent advances in nanoindentation. The nanomechanical properties of byssal cuticle were determined from embedded threads microtomed at one end to prepare a smooth surface. Hydrated cuticle sections were assessed by manual or programmed indentation for hardness and stiffness (47, 48). Thread sections enable hardness and stiffness measurements for the collagen core as well as for the cuticle. In *M. californianus*, core stiffness and cuticle stiffness are 0.5 GPa and 2.5 GPa, respectively. Hardness (H), in contrast, is 0.1 versus 0.5 GPa for core and cuticle, respectively. These values are worth comparing with those of the hardest known epoxies, for which average H is 0.5 GPa. In short, despite a thread extensibility of 70–100%, the cuticle is four to six times harder and stiffer than the core—a good albeit peculiar hedge against wear.

A rubber band coated by a layer of paraffin also has a protective sheath approximately five to six times harder than the core, but stretching the rubber band once to double its initial length shatters the coating. The cuticle of *Mytilus* threads does not shatter at high strains (less than 100% in *M. californianus*), and therein rests its real value (Figure 8a): Stiff synthetic coatings with high strain capacity have yet to be invented. Even among marine mussels, the talent appears limited to *Mytilus*. A New Zealand mussel, *Perna canaliculus*, has strong threads and a hard cuticle, but extension to only 30% causes catastrophic cracking

(48). Perhaps *Perna*'s cuticle is less adapted because high thread extension is rarely encountered in its subtidal habitat.

3.4.2. Microstructure—Ultrastructural analyses sought a structural explanation for hard cuticles with high strain capacity after the application of various strains. The examination of unloaded *M. galloprovincialis* cuticle by TEM revealed a composite structure in which roughly spherical inclusions (of diameter 800 nm) are dispersed in a continuous and homogeneous matrix (Figure 8b). The volume fraction of each is 0.5 (47). The inclusions known as granules in the literature have peculiar marbled microarchitectures. During loading, the granule aspect ratio changes, and granules elongate to almost 1.2 at 30% strain, after which there is no further change. Apparent in the microstructure of cuticle beyond 30% strain is a subtle network of microcracks usually at the interface between matrix and granules. The microcracks resist coalescence into larger cracks until strains of 70% and 100% in *M. galloprovincialis* and *M. californianus*, respectively, are reached (47).

Given that stress concentration occurs whenever granules are not uniformly surrounded by matrix, cuticle fabrication is a topic of increasing interest. Byssal cuticle formation has been investigated in detail only once, by Vitellaro Zuccarello (49) in what she termed the “enzyme gland” (also known as the accessory gland) of the foot in *M. galloprovincialis*. The process begins like any secretory pathway, with a condensing vacuole in which protein is accumulated and gradually organized. Once granules are complete, they are encircled by a generous halo of matrix and are then ready for secretion. After assembly of a new byssal core in the foot groove, the haloed granules are released en masse by the enzyme gland and coalesce to engulf the thread.

3.4.3. Proteins—Only one protein, mfp-1, is associated with certainty with byssal cuticles (50). Other ingredients include calcium, iron, and perhaps fatty acids (51). Mfp-1 is a large (~108 kDa in *M. edulis*) and basic (isoelectric point = 10.5) protein that consists of a tandemly repeated decapeptide motif with a mature consensus sequence of A-K-O-S-Y*-O*-O-T-Y*-K (where O is *trans*-4-hydroxyproline, O* is *trans*-2,3-*cis*-3,4-dihydroxyproline, and Y* is Dopa) (Table 1) (52, 53). Surface behavior and solution properties of this protein have been thoroughly investigated and reviewed (46, 54). Briefly, mfp-1 has an open and extended structure in solution with some evidence for a left-handed 3_1 helix. The presence of 15-mol% Dopa makes it prone to oxidation, especially at or above neutral pH; however, oxidation has been observed at pH as low as 5.5 (54).

The most pronounced chemical reactivity of mfp1 is the complexation or chelation of Fe^{3+} . At pH of 7.5, iron chelation is evident by a red color (500 nm) associated with tris-catecholato-iron(III) formation (39). By control of the Fe^{3+} :Dopa ratio, the color can be shifted from red (low) to purple (high). The red color in particular is associated with strong charge transfer from the nonbonding π orbitals of Dopa oxygen to empty *d* orbitals of iron (55). The relevance of this chemistry in byssus has been confirmed by in situ electron paramagnetic resonance (40) and more dramatically by Raman microscopy (Figure 8c,d) (38). The charge transfer associated with Dopa-Fe(III) complexes in the cuticle results in strong resonance Raman signals that can be used for mapping the distribution of these interactions with micrometer resolution (Figure 8e).

At higher magnification, resonance Raman microscopy reveals an intriguing detail about the fine structure of byssal cuticle in *M. galloprovincialis*. The signal intensity at 500 to 650 cm^{-1} , the frequency of catechol-O-Fe(III) stretching, is twice as intense in the granules as in the matrix (38). Although mfp-1 is distributed throughout the cuticle, it is perhaps more densely bundled in the granules than in the matrix. This is possible if mfp-1 exists in two different physically separated states: high Dopa (20 mol%) and low Dopa (10 mol%), where

the former may be associated with the granule and the latter with the haloes. The higher iron content is presumably recruited by the compartment, e.g., a mfp-1 variant, with the greater Dopa content. Other explanations are possible.

The ability of mfp-1 to interact with surfaces has been addressed using a number of different analytical techniques. These were reviewed recently (46) and need not be revisited here. Lin et al. (18) were the first to distinguish the behavior of mfp-1 from that of other mfps on mica surfaces. Mfp-1 films bind tightly to both mica surfaces in the SFA, as exhibited by the reversibly compressible hard wall at 5 nm, but by themselves they are not inclined to bridge from one surface to another, as does mfp3. The coating but not the bridging mode on surfaces was consistent with a protein that provides the cuticle with a natural coating on the byssus. With a thickness of approximately 5 μm , however, the cuticle has room for hundreds of mfp1 layers with a thickness of 5 nm each. Unless these layers have some way of interacting from molecule to molecule, there is little cohesive strength. Fe^{3+} at 10- μM solutions at pH 5.5 mediates bridging between mfp-1 layers, but the effect is concentration dependent, as 100- μMFe^{3+} abolishes bridging (56) (Figure 9). The Fe^{3+} -to-Dopa ratio apparently influences whether one, two, or three Dopas bind to each metal nucleus. Protein cross-links occur only when two or three Dopas come together.

3.5. Conclusion: Sizing Up the Biology

The byssal plaques of mussels are exquisitely adapted for attachment to wet surfaces. Architecturally, they are hierarchically organized with a hard but extensible outer coating, gradient porous core, and fiber reinforcement for intimate union with the byssal thread collagens. The diverse plaque architecture is matched by a diverse protein composition, of which five to six proteins are localized exclusively to the plaque. Proteins such as mfp-3 and mfp-5 in the primer or front line of adhesion are enriched with up to 30-mol% Dopa; the side chain is exploited for robust bidentate interactions with surfaces, and W_A is as high as 7 mJ m^{-2} on mica. Potent antioxidants such as mfp-6 are available to keep a certain proportion of the interfacial Dopa reduced for good adsorption. Mfp-6, however, is also adapted to function as a cross-linker once its reducing power is depleted, forming S-cysteiny-Dopa adducts. Evidence for covalent cross-linking between mfps based on aryl coupling also exists, e.g., that in 5,5'-di-Dopa (57), but the extent to which quinone cross-linking contributes to plaque cohesion is still open to question. Three factors that favor the formation of cross-links in byssus are the facile auto-oxidation of Dopa to Dopakinone, the redox exchange between Fe^{3+} and Dopa (40), and the presence of catecholoxidase activity (58). Recent SFA analyses suggest that notions about protein cohesion in the plaque must be expanded to include Ca^{2+} and Mg^{2+} ion bridging (mfp-2 \leftrightarrow mfp-2), chelate complexes with Fe^{3+} (mfp-1 \leftrightarrow mfp-1 and mfp-2 \leftrightarrow mfp-2), and strong intrinsic protein-protein binding complexes such as those between mfp-2 and mfp-5 and between mfp-3 and mfp-5.

4. MUSSEL-INSPIRED SYNTHETIC POLYMERS

4.1. Motivation and General Design Features

Due to their exceptional adhesive performance in wet and turbulent environments, mussel byssal proteins represent attractive targets for biomimetic efforts. Biomimetic constructs offer the obvious opportunity to capture the functional properties of native proteins in synthetic systems as well as to further elucidate the properties of native proteins. Efforts in this area have thus far been dominated by relatively simple peptide and polymer constructs containing Dopa or the catechol functional group found in Dopa, as Dopa is now accepted as being an essential component of many byssal proteins, with both cohesive and adhesive roles (see Section 3.3.4). With further time and research, the compositional space of biomimetic systems will certainly expand to reflect what is discovered about the role of

other byssal protein residues (phosphoserine, lysine, histidine, hydroxyarginine, etc.) and the complex interplay between these residues and Dopa.

Figure 10 schematically shows prototypical configurations of mussel mimetic synthetic polymers. The earliest examples of mussel mimetic polymers were Dopa polypeptides chemically synthesized by solid- or solution-phase peptide chemistry (59–62). Later, Dopa and lysine polypeptide copolymers were developed by ring-opening polymerization of *N*-carboxyanhydride monomers (63–65). Recombinant DNA technologies have also been employed to create adhesive proteins (66–68). Protein- and polypeptide-based adhesives have been reviewed (69–71). In this review we instead focus on synthetic mussel mimetic polymers.

One frequent synthetic approach is to functionalize linear or branched polymers with Dopa, Dopa peptides, or other catechol functional groups by employing standard chemical ligation chemistries. This approach is exemplified by a family of poly(ethylene glycol) (PEG)-based linear and branched polymers in which Dopa was incorporated as a terminal group on each polymer chain (Figure 10) (72, 73). Alternatively, one may directly synthesize polymers through polymerization of Dopa or a catechol-based monomer. Although one must be careful to avoid partial inhibition of free-radical polymerization by catechols in the presence of atmospheric oxygen, several recent reports of free-radically polymerized catechol polymers attest to the viability of this approach (74–80). Combinations of monomers give rise to a tremendous potential composition and property space and are nicely exemplified by copolymers derived from polymerization of Dopamine methacrylamide (DMAM) with 2-methoxyethyl acrylate (MEA) or poly(ethylene glycol) methyl ether methacrylate (mPEG-MA) (81). The resulting copolymers have highly divergent physical properties and can be used as adhesive, e.g., p(DMAM-*co*-MEA), or nonadhesive, e.g., p(DMAM-*co*-mPEG-MA), coatings, where p(DMAM-*co*-MEA) denotes poly(Dopamine-methacrylamide-*co*-2-methoxyethyl acrylate) and p(DMAM-*co*-mPEG-MA) denotes poly[Dopamine-methacrylamide-*co*-poly(ethylene glycol)-methylether methacrylate], respectively (Figure 11). Other examples of free-radically polymerized mussel mimetic polymers have been reported. Polymers derived from the catecholic monomer 3,4-dihydroxystyrene have been synthesized, as have copolymers of this monomer with styrene or styrene sulfonate (78–80, 82, 83). Copolymers provide access to a wide range of physical properties through readily accessible starting materials and preparation methods suitable for mass production. The catechol content of most synthetic polymers described in the literature ranges from a few mol% to 30 mol% or more and therefore lies within the general range of catechol content found in native mussel adhesive proteins.

4.2. Synthetic Polymers and the Role of Dopa in Interfacial Adhesion

Synthetic polymers used in combination with specialized adhesion methodologies can yield additional insights into certain aspects of mussel adhesion. These studies employ simple polymer designs containing short peptides or even single amino acids and as such should be considered very simple model systems that lack the full complexities of native proteins. Nevertheless, these approaches can isolate and probe the contributions of key protein residues.

Molecular-level studies of Dopa interfacial behavior were performed by grafting a single Dopa residue to an atomic force microscope (AFM) cantilever via a PEG tether and by measuring the force required to pull the molecule from contact with a substrate (84). These measurements revealed strong and reversible interactions between Dopa and metal oxides, likely due to the formation of bidentate metal-oxygen coordination bonds between the Dopa catechol and surface metal atoms of the oxide. For titanium oxide, single-molecule pull-off forces of >500 pN have been measured in the presence of water, suggesting the ability of

Dopa to outcompete water for interaction with the oxide surface. The strength of the interaction between Dopa and an oxide surface appears to be highly pH dependent, as measurements performed at high pH resulted in significantly attenuated pull-off forces. Auto-oxidation of Dopa to Dopaoquinone at alkaline pH is likely responsible for this observation, implying that the interaction with titanium oxide is stronger in the catechol form compared with quinone. This is not to say that Dopaoquinone is unlikely to contribute to interfacial bonding. Specifically, interactions with organic surfaces may benefit from covalent reactions between quinones and nucleophiles commonly present on organic surfaces. Single-molecule studies performed at high pH resulted in covalent bond formation between Dopa and primary amine surfaces. Although the exact reaction mechanism is uncertain, likely candidates include Michael addition or Schiff base reactions with primary amines on the surface. Single-molecule studies of Dopa interacting with mucin revealed strong non covalent interactions (85). Although the nature of the interactions was not determined, the single-molecule results were in qualitative agreement with an observed increase in mucoadhesion upon functionalization of Dopa with PEG (85).

Bridging the length scales between single-molecule and macroscopic experiments are micromechanics measurements, for example, contact mechanics approaches conducted on Dopa-containing hydrogels. Shull and colleagues (86–88) and Deruelle et al. (89) have utilized these methods to probe the influence of Dopa and its oxidation state on adhesion to inorganic and organic surfaces. In these experiments, typically an elastic gel hemisphere is brought into contact with a solid surface and then retracted while the contact area and force are measured (90), allowing the influence of Dopa and its oxidation state on adhesion to inorganic and organic surfaces to be studied. These methods offer distinct advantages over the lap shear and tensile adhesion tests that have been far more widely employed to determine the adhesive properties of Dopa-containing materials (64, 91, 92). Macroscopic test methodologies cannot easily differentiate between cohesive and adhesive contributions to the measured values, and bulk mechanical properties can significantly alter the performance of an adhesive in these test methods (93). In recognition that oxidation and interfacial binding typically occur simultaneously during byssus formation and that Dopa likely has multiple roles in this process, it is important to employ methods that allow for discrimination between cohesive and adhesive contributions of Dopa.

To elucidate Dopa's interfacial binding role in the absence of oxidation, Lee et al. (94) incorporated Dopa in its reduced form into photocured hydrogels that did not utilize oxidation in the curing process. Load-versus-displacement contact curves (Figure 12) of a Dopa-modified gel hemisphere showed significant hysteresis on a titania (TiO_2) surface underwater compared with control (Dopa-free) gels (94). W_A or the energy required to separate the gel from TiO_2 increased with increasing Dopa content, indicating that catechol enhances adhesion with the metal oxide surface. To study the effect of Dopa oxidation on adhesion, preformed Dopa-containing gels were treated with periodate prior to contact with the substrate. Oxidation significantly reduced W_A between Dopa-modified gels and the TiO_2 substrate. By controlling the oxidation state of Dopa, this experimental model demonstrated that the adhesive properties of Dopa toward metal oxides decrease with oxidation.

Guvendiren and coworkers (95) subsequently explored the interfacial binding properties of Dopa-modified block copolymer membranes with tissue surfaces as a function of the oxidation state of the catechol. The investigators utilized a new pressure-controlled membrane contact configuration. In this configuration, application of a positive pressure forced the membrane into contact with the surface of interest, after which a negative pressure was applied to separate the membrane from the substrate. The release pressure (P_R) was used as a measure of the strength of the adhesive interaction. The membrane geometry is well suited for rough or chemically heterogeneous surfaces (i.e., tissue surfaces). Thus,

the method was used to characterize the adhesive interaction of Dopa with pigskin (Supplemental Figure 1; follow the **Supplemental Material link** from the Annual Reviews home page at <http://www.annualreviews.org>). Although Dopa-modified membrane was adhesive to submerged tissue, P_R increased dramatically when a periodate solution was added while the membrane was in contact with the tissue. Presumably, in situ oxidation of Dopa to highly reactive Dopaquinone resulted in covalent bond formation with functional groups (i.e., $-\text{NH}_2$ or $-\text{SH}$) present on the tissue surface.

These experiments as well as the SFA results described in Section 3.3.4 yield a picture of remarkable interfacial chemical versatility in which Dopa appears adept at adhesive interactions with both inorganic and organic surfaces. These interactions can be either covalent or noncovalent. Mechanistic understanding of Dopa in oxidative cross-linking and interfacial binding serves as a guide in designing novel biomimetic adhesive materials. In the following section we provide some examples of mussel mimetic materials being developed for use in the medical clinic.

4.3. Synthetic Medical Polymer Adhesives and Sealants

An obvious application for mussel adhesive protein mimetic polymers is as adhesives that bind together surfaces or seal holes in materials. Injectable wet medical adhesives capable of bonding or repairing tissues are considered one of the frontier areas in this realm. However, there are great challenges associated with adhering in the presence of excess biological fluid, as well as the usual concerns related to the biological response to synthetic polymers. For medical applications, a rapid sol-gel transition in the presence of tissue is desired so as to minimize surgical delay. This would typically be accomplished by administration of a liquid polymer solution, preferably aqueous, that solidifies within seconds or tens of seconds in vivo. The real opportunity here lies in exploiting the chemical properties of the catechol to generate cohesive and adhesive strength in the solidified adhesive.

In the Dopa-modified PEG polymers shown in Supplemental Figure 2, the nonreactive PEG polymers serve as inert and biocompatible macromolecular supports to which cohesive and adhesive characteristics are imparted by introducing Dopa (72). Solutions of branched and linear PEGs with Dopa end groups readily formed hydrogels when treated with either chemical (periodate) or enzymatic (horseradish peroxidase and mushroom tyrosinase) oxidants. The rate of curing was dependent on the type and concentration of oxidant, with gel formation requiring between 30 s and several hours. For periodate-cured gels, curing was fastest at approximately equimolar periodate and Dopa, whereas the curing rate for enzyme-mediated oxidation decreased exponentially with increasing enzyme concentration. These observations were attributed to differences in the cross-linking pathway, as cross-link formation proceeded by either quinone methide tanning (periodate) or phenol coupling (enzymatic) pathways. Model studies involving molecular weight characterization of oxidized linear monofunctional methoxy-PEG-Dopa revealed the formation of oligomers of methoxy-PEG-Dopa resulting from oxidative cross-linking of up to six Dopa end groups (72), indicating that Dopa-Dopa cross-linking is responsible for network formation in multifunctional linear and branched PEG-Dopa polymers.

Several PEG-based mussel mimetic polymers have demonstrated strong adhesion to tissue (91, 96, 97). These adhesives outperform fibrin glue in various macroscopic adhesion tests, including lap shear, burst strength, and peel adhesion tests. By control of variables such as PEG architecture, molecular weight, number of terminal Dopa residues (up to four), and linking group (e.g., ester, urethane, amide), adhesives with a variety of properties (e.g., rate of curing, extent of swelling, mechanical properties, and degradation rate) can be obtained. For example, complete hydrogel degradation times ranging from 26 h to more than 3 months can be achieved without affecting the adhesive performance of these adhesives. Other

catechol-containing molecules such as Dopamine or 3,4-dihydroxyhydrocinnamic acid impart adhesive and cross-linking ability in a similar fashion when used in place of Dopa on the PEG polymer (96, 97). PEG-catechol adhesives are being developed to have handling properties similar to those of other PEG-based medical sealants that are commercially available [e.g., CoSeal (Baxter International) and DuraSeal (Confluent Surgical)]. Such adhesives are envisioned to be deployed in a clinical setting as a two-component system delivered via a double-barrel syringe or similar device.

The *in vivo* performance of PEG-catechol adhesives was recently investigated in mice (73). The purpose of this work was to demonstrate mussel-inspired adhesive performance *in vivo*, with an emphasis on tissue biocompatibility and integrity of the adhesive-tissue interface. Rapid gelling mixtures of periodate and a nondegradable four-arm PEG-catechol were applied onto adipose tissue surfaces, where they formed adherent hydrogel coatings *in situ*. Histological evaluation at time points up to 1 year after implantation showed minimal inflammatory cell infiltrate and little evidence of fibrotic capsule formation (Figure 13*a*). At all observed time points, the adhesive hydrogel material was visible and present at the original deposition site, and the material-tissue interface was intact. The surrounding adipose tissue was healthy and well vascularized, and there was no evidence of nonspecific postsurgical adhesions. A more stringent test of biocompatibility consisted of transplanting mouse islets onto adipose and liver surfaces of diabetic mice using PEG-catechol hydrogel; the adhesive was designed to seal the islets directly onto the tissue surface in a minimally invasive manner. The adhesive formed a visible, translucent, thin hydrogel layer over the affixed islet bolus, resulting in islet entrapment between the adhesive and tissue surface. Blood glucose was used as a measure of islet graft performance and adhesive biocompatibility. Control mice and those transplanted with PEG-catechol adhesive showed no statistical difference in the mean number of days posttransplant after which normoglycemia was achieved. Histological analysis of the implant site revealed PEG-catechol-immobilized islets to be well vascularized after several months *in vivo* (Figure 13*b*) and to actively secrete insulin. This result is promising, given the high sensitivity of islets to chemical and physical insults, indicating that the PEG-catechol adhesive material does not interfere with islet engraftment to the host tissue.

Recently, a mussel mimetic polymer adhesive was investigated as a candidate injectible surgical sealant for repair of gestational fetal membrane ruptures (98). Invasive diagnostic and therapeutic fetal surgical procedures performed endoscopically require access with large-diameter fetoscopes and are frequently complicated by amniotic fluid leakage, separation of amnion and chorion, or iatrogenic preterm premature rupture of the fetal membranes (iPPROM). The morbidity and mortality associated with iPPROM may compromise the expected benefits of the intervention and are therefore potentially serious complications for prenatal fetal surgery. A material capable of plugging membranes after established rupture or as a prophylactic to prevent leakage at fetoscopic access sites is greatly needed. Such a material would ideally present an immediate, nontoxic, and durable physical barrier to amniotic fluid and would be capable of application to wet tissue surfaces.

PEG-catechol and several other sealants (DERMABOND, Histoacryl, Tissucol fibrin glue, and two other types of *in situ*-forming, PEG-based polymer hydrogels) were tested for acute toxicity upon direct contact with human fetal membranes for 24 h of organ culture. Bonding and toxicity were assessed through tissue histomorphological analysis of 3.5-mm membrane defects created with a trocar and were then sealed with PEG-catechol adhesive (Figure 14). The sealed defects were further tested for mechanical integrity and were found to provide leak-proof closure that withstood membrane stretch in an *in vitro* model. Acute toxicity was assessed by direct application of sealant onto human fetal membranes followed by 24 h of organ culture. Only Tissucol and the PEG-catechol adhesive showed efficient,

nondisruptive, and nontoxic bonding to fetal membranes. Other PEG-based adhesives either were poorly adhesive to the tissue or were not detected after 24 h, whereas cyanoacrylate medical adhesives elicited a highly aggressive adverse tissue response (Supplemental Figure 3). On the basis of these preliminary studies, synthetic PEG-catechol tissue adhesives have emerged as a potential sealing modality for fetal membrane defects and merit further evaluation *in vivo*.

Stewart and coworkers (77) recently described synthetic mimics of glues secreted by the sandcastle worm *P. californica*. Like mussels, these organisms employ Dopa-containing proteins for their glues. In sandcastle worm glue, complex coacervates may be formed from mixtures of weakly acidic and weakly basic proteins (42). The authors mimicked this system in the form of a catechol-containing synthetic polyanion, which, when combined with a synthetic polycation at specific ionic strength and pH, formed a complex coacervate adhesive (77). The liquid adhesive could be cross-linked into a solid through addition of a chemical oxidant, and this strategy was employed for *in vitro* bonding of bone fragments (Figure 15). The authors subsequently reported a related environmentally triggered system that exhibited good *in vitro* bond strength to bone (43) and was recently adapted for the adhesive reconstruction of a cranial fracture in a rat model system (99).

4.4. Synthetic Polymers Used as Coatings

The strong surface adhesion of Dopa offers many opportunities for the development of novel polymer coatings useful in a variety of ways. Depending on architecture and composition, the catechol may serve as an anchor in immobilizing a polymer coating onto a surface or may impart adhesive value to the applied coating.

One interesting use for p(DMAm-*co*-MEA) is as a coating for enhancing wet adhesion of reversible fibrillar adhesive mimics of gecko foot hairs (75, 76). The fibrillar attachment mechanisms of geckos, flies, and other organisms are believed to rely upon weak intermolecular forces and typically function poorly in the presence of excess water (see discussion in Section 2). Borrowing ideas from the wet adhesive proteins found in mussel holdfasts, Lee and coworkers (76) devised a hybrid biologically inspired adhesive consisting of an array of nanofabricated polymer pillars coated with a thin layer of p(DMAm-*co*-MEA) (Figure 16). Wet adhesion of the nanostructured polymer pillar arrays increased nearly 15-fold when coated with mussel adhesive protein mimetic polymer. The adhesive functioned like a wet/dry sticky note, maintaining its adhesive performance for more than 1,000 contact cycles in both dry and wet environments. This hybrid adhesive, which uniquely combines the salient design elements of both gecko and mussel adhesives, may prove useful for reversible attachment to a variety of surfaces in many environments.

A significant amount of research has been performed on antifouling polymer coatings in which PEG and other polymers are grafted onto surfaces via catechol functional groups (84, 100). These coatings may be formed by either graft-to or graft-from approaches and range in thickness from a few nanometers to >100 nm (Figure 17). At sufficiently high antifouling polymer surface density, the adhesion of protein, cells, bacteria, and algae is significantly reduced compared with unmodified surfaces. The first manifestation of this approach consisted of a PEG coupled to a decapeptide sequence derived from mfp-1 (Table 1). Researchers later discovered that such sophisticated constructs are unnecessary and may be simplified down to a single catechol or a few catechols interspersed with amine groups (e.g., lysine). A highly reductionist approach involves the use of low-molecular-weight catecholamines that polymerize at alkaline pH to produce thin adherent coatings onto which antifouling polymers may be grafted (Figure 18) (101).

PEG with a Dopa tripeptide anchor on one end group (mPEG-Dopa₃) was effective at preventing bacterial attachment and subsequent biofilm formation on a variety of surfaces (102, 103). mPEG-DOPA₃-coated titanium surfaces demonstrated a greater-than-94% reduction in bacteria binding over uncoated surfaces when challenged with 10⁵ colony-forming units (CFU) ml⁻¹ of six major uropathogenic bacterial strains for 24 h at 37°C in human pooled urine. A >231-fold reduction in adherence for *Escherichia coli* GR-12, *Enterococcus faecalis* 23241, and *Proteus mirabilis* 296 compared with uncoated TiO₂ disks was observed (Supplemental Figure 4) (102). Scanning electron microscopy also reflected these results and demonstrated the ability of the coating to resist urinary constituent adherence. Similar catechol-modified PEG coatings also demonstrated a significant reduction in bacteria adhesion when coated onto common catheter and stent materials (e.g., polyurethane and silicone rubber) (103).

A subsequent in vivo study in a rabbit model with uropathogenic *E. coli* cystitis was performed with urinary stent curls coated with p(DMAM-co-mPEG-MA) (104). In this model, uncoated and coated devices were inserted transurethraly into the bladders of male New Zealand white rabbits, followed by instillation of uropathogenic *E. coli* strain GR-12 (10⁷ CFU) and examination of their urine for bacteria for up to 7 days. p(DMAM-co-mPEG-MA)-coated devices showed decreased urine bacterial counts compared with those in uncoated catheters; eight of ten rabbits demonstrated sterile urine by day 3. The p(DMAM-co-mPEG-MA) coating strongly resisted bacterial attachment, resulting in improved infection clearance over that of uncoated devices.

If desired, bioactive functional groups can be presented in such coatings over a background of antifouling polymer to resist nonspecific interactions. For example, DOPA₃-PEG-biotin coatings facilitate biofunctionalization with peptides and other biomolecules via biotin-avidin interactions. This was demonstrated for cell binding peptide ligands for α5β1 [cyclic RGD (cRGD)] and α4β1 [cyclic LDV (cLDV)] (105). Hematopoietic M07e cells bound specifically to immobilized cRGD and cLDV integrins in a dose-dependent manner, opening the door to incorporating biospecific functional groups into such coatings (Figure 18).

Researchers in this field are also beginning to move beyond PEG and to explore other antifouling polymers with catechol anchors. For example, a new family of *N*-substituted glycine polymers (peptoids) is being investigated as candidate antifouling polymers (106–108). These polymers have a polypeptide backbone, with natural or unnatural side chains substituting from the amide nitrogen as opposed to the alpha carbon. Investigators have explored a number of side-chain chemistries, including methoxyethyl, methoxypropyl, and hydroxypropyl, that demonstrate good protein, cell, and bacterial adhesion resistance. Other examples include zwitterionic polymers (71, 109, 110) and biopolymers (111–113) bound to solid surfaces using catechol functional groups.

4.5. Nanoparticle Stabilization

Finally, catechol anchors work equally well for attaching polymers onto surfaces of nanoparticles, including those envisioned for medical applications (114–118). An interesting recent development in this area relates to an investigation of the stability of catechol anchors under physiological conditions (120). In this study, PEG was anchored onto iron oxide nanoparticles by a variety of substituted catechols, and thermal and salt stability was determined. Nitro-substituted Dopa and Dopamine demonstrated enhanced stability of iron oxide nanoparticles. These nanoparticles could be repeatedly heated up to 90°C without noticeable agglomeration, whereas catechols with lower affinity resulted in irreversible agglomeration. The enhanced binding of nitrocatechol to iron oxide may be attributed to the lower p*K*_a (~6.5) dissociation constant of the first catechol hydroxy group compared with unsubstituted catechols like Dopa (p*K*_a > 9). 2-Nitrocatechol forms a more stable complex

with TiO₂ than does catechol (119, 120). The effect of phenol pK_a on the binding strength of the catechol may represent yet another attribute that is already exploited in nature and from which a biomimetic approach can learn. Recently, Sun et al. (121) detected chlorinated Dopa (2-chloro-4,5-dihydroxyphenylalanine) in adhesive proteins secreted by sandcastle worm. These investigators proposed that halogenated Dopa was utilized as a mechanism to increase oxidation potential of the adhesive molecule, thus preserving its reduced and more adhesive form compared with the oxidized Dopakinone. Further studies in this area may lead to enhanced catecholic anchors for coatings.

5. CONCLUSIONS

Mussel adhesion protein-inspired polymer research is motivated by the idea that the exceptional adhesive properties exhibited by the native proteins can be captured in synthetic polymer systems. A variety of chemical approaches may be employed, giving rise to linear or branched polymers functionalized with Dopa, Dopa peptides, or their catechol mimics. These polymers provide simple platforms for studying the role of Dopa in mussel adhesion as well as novel materials for wet adhesion. One of the compelling uses for these materials is in medical adhesion and sealing, in which catechols enhance adhesion to wet tissue surfaces. Progress is being made toward the development of mussel mimetic polymers capable of repairing both soft and hard tissues. Finally, there is rapid adoption of mussel mimetic polymers in the coatings field. Here, the adhesive qualities of the catechol may be important for anchoring polymers, biomolecules, and other compounds onto solid surfaces. With careful design of polymer composition and architecture, these coatings can give rise to adhesive or antiadhesive coatings.

Supplementary Material

Refer to Web version on PubMed Central for supplementary material.

Acknowledgments

We acknowledge the Human Frontiers of Science Program and the National Institutes of Health for funding. We thank S. Jewhurst for preparing freeze-fractured plaques and W. Wei, J. Yu, E. Danner, and M. Hammer for sharing unpublished data. J. N. Israelachvili and J.H. Waite are responsible for Sections 1 to 3 of the review, whereas B.P. Lee and P.B. Messersmith wrote Sections 4 to 5.

LITERATURE CITED

1. Comyn, J. The relationship between joint durability and water diffusion. In: Kinloch, A.J., editor. *Developments in Adhesives*. Vol. 2. Appl. Sci. Publ.; Barking, UK: 1981. p. 279-313.
2. Israelachvili, J.N. *Intermolecular and Surface Forces*. 3rd ed. Elsevier; London: 2010.
3. Gutmann V. Solvent effects on the reactivities of organometallic compounds. *Coord. Chem. Rev.* 1976; 18:225–55.
4. Clint JH, Wicks AC. Adhesion under water: surface energy considerations. *Int. J. Adhes. Adhes.* 2001; 21:267–73.
5. Pocius, AV. *Adhesives and Adhesives Technology*. Hanser/Gardner Publ.; Cincinnati: 1997.
6. Waite JH, Holten-Andersen N, Jewhurst SA, Sun CJ. Mussel adhesion: finding the tricks worth mimicking. *J. Adhes.* 2005; 81:297–317.
7. Silverman HG, Roberto FE. Understanding mussel adhesion. *Mar. Biotechnol.* 2007; 9:661–81. [PubMed: 17990038]
8. Harris, VA. *Sessile Animals of the Seashore*. Chapman & Hall; London: 1990.
9. Hawkins AJS, Bayne BL. Seasonal variation in the relative utilization of carbon and nitrogen by the mussel *Mytilus edulis*: budgets, conversion efficiencies and maintenance requirements. *Mar. Ecol. Prog. Ser.* 1985; 25:181–88.

10. Griffiths CL, King JA. Energy expended on growth and gonad output in the ribbed mussel *Aulacomya ater*. *Marine Biol.* 1979; 53:217–22.
11. Waite JH. The formation of mussel byssus: anatomy of a natural manufacturing process. *Results Probl. Cell Differ. (Biopolymers)*. 1992; 19:27–54.
12. Aldred N, Ista LK, Callow ME, Callow JA, Lopez GP, et al. Mussel (*Mytilus edulis*) byssus deposition in response to variations in surface wettability. *J. R. Soc. Interface.* 2006; 3:37–43. [PubMed: 16849215]
13. Crisp DJ, Walker G, Young GA, Yule AB. Adhesion and substrate choice in mussels and barnacles. *J. Colloid Interface Sci.* 1985; 104:40–50.
14. Bell EC, Gosline JM. Mechanical design of mussel byssus: Material yield enhances attachment strength. *J. Exp. Biol.* 1996; 199:1005–17. [PubMed: 9318809] Classic study of the organismal design of byssus in mussels.
15. Bell EC, Gosline JM. Strategies for life in flow: tenacity, morphometry, and probability of dislodgment of two *Mytilus* species. *Mar. Ecol. Prog. Ser.* 1997; 159:197–208.
16. Allen JA, Cook M, Jackson DJ, Preston S, Worth EM. Observations on the rate of production and mechanical properties of the byssus threads of *Mytilus edulis* L. *J. Molluscan Stud.* 1976; 42:279–89.
17. Burkett JR, Wojtas JL, Cloud JL, Wilker JJ. A method for measuring the adhesion strength of marine mussels. *J. Adhes.* 2009; 85:601–15.
18. Lin Q, Gourdon D, Sun CJ, Holten-Andersen N, Anderson TH, et al. Adhesion mechanisms of the mussel foot proteins mfp-1 and mfp-3. *Proc. Natl. Acad. Sci. USA.* 2007; 104:3782–86. [PubMed: 17360430]
19. Tamarin A, Lewis P, Askey J. Structure and formation of byssus attachment plaque in *Mytilus*. *J. Morphol.* 1976; 149:199–221. [PubMed: 933173] Detailed study of plaque structure and formation in mussel byssus.
20. Lappin-Scott HM, Costerton JW. Bacterial biofilms and surface fouling. *Biofouling.* 1989; 1:323–42.
21. Waite JH, Lichtenegger HC, Stucky GD, Hansma P. Exploring the molecular and mechanical gradients in structural bioscaffolds. *Biochemistry.* 2004; 43:7653–62. [PubMed: 15196007]
22. Inoue K, Takeuchi Y, Miki D, Odo S. Mussel adhesive plaque protein is a member of epidermal growth factor like gene family. *J. Biol. Chem.* 1995; 270:6698–701. [PubMed: 7896812]
23. Rzepecki LM, Hansen KM, Waite JH. Characterization of a cystine-rich polyphenolic protein family from the blue mussel *Mytilus edulis* L. *Biol. Bull.* 1992; 183:123–37.
24. Hwang DS, Zeng H, Harrington MJ, Masic A, Israelachvili JN, et al. Protein- and metal-dependent interactions of mfp-2, the dominant protein of mussel adhesive plaques. *J. Biol. Chem.* 2010; 285:25850–58. [PubMed: 20566644]
25. Florioli RY, von Langen J, Waite JH. Marine surfaces and the expression of specific byssal adhesive protein variants in *Mytilus*. *Mar. Biotechnol.* 2000; 2:352–63. [PubMed: 10960125]
26. Papov VV, Diamond TV, Biemann K, Waite JH. Hydroxyarginine-containing polyphenolic proteins in the adhesive plaques of the marine mussel *Mytilus edulis*. *J. Biol. Chem.* 1995; 270:20183–92. [PubMed: 7650037]
27. Zhao H, Robertson NB, Jewhurst SA, Waite JH. Probing the adhesive footprints of *Mytilus californianus* byssus. *J. Biol. Chem.* 2006; 281:11090–96. [PubMed: 16495227]
28. Zhao H, Waite JH. Proteins in load bearing junctions: histidine-rich metal binding protein of mussel byssus. *Biochemistry.* 2006; 45:14223–31. [PubMed: 17115717]
29. Waite JH, Qin XX. Polyphenolic phosphoprotein from the adhesive pads of the common mussel. *Biochemistry.* 2001; 40:2887–93. [PubMed: 11258900]
30. Zhao H, Waite JH. Linking adhesive and structural proteins in the attachment plaque of *Mytilus californianus*. *J. Biol. Chem.* 2006; 281:26150–58. [PubMed: 16844688]
31. Yu J, Wei W, Danner E, Ashley RM, Israelachvili J, Waite JH. Antioxidant is a key factor in mussel protein adhesion. *Nat. Chem.* 2011 In revision.
32. Qin XX, Coyne KJ, Waite JH. Tough tendons: Mussel byssus has collagen with silk-like domains. *J. Biol. Chem.* 1997; 272:32623–27. [PubMed: 9405478]

33. Qin XX, Waite JH. A collagenous precursor that may mediate block copolymer gradients in mussel byssal threads. *Proc. Natl. Acad. Sci. USA*. 1998; 95:10517–22. [PubMed: 9724735]
34. Harrington M, Waite JH. Holdfast heroics: comparing *Mytilus californianus*. *J. Exp. Biol.* 2007; 210:4307–18. [PubMed: 18055620]
35. Sagert J, Waite JH. Hyperunstable matrix proteins in the byssus of *Mytilus galloprovincialis*. *J. Exp. Biol.* 2009; 210:2224–36. [PubMed: 19561212]
36. Benedict CV, Waite JH. Location and analysis of byssal structural proteins of *Mytilus edulis* L. *J. Morphol.* 1984; 189:171–82. [PubMed: 3018262]
37. Anderson KE, Waite JH. Immunolocalization of Dpfp1, a byssal protein of the zebra mussel (*Dreissena polymorpha*). *J. Exp. Biol.* 2000; 203:3065–76. [PubMed: 11003818]
38. Harrington MJ, Masic A, Holten-Andersen N, Waite JH, Fratzl P. Iron-clad fibers: a metal-based biological strategy for hard flexible coatings. *Science*. 2010; 328:216–20. [PubMed: 20203014] Raman microscopy for localizing Fe³⁺ coordination by Dopa in byssus.
39. Taylor SW, Chase DB, Emptage MH, Nelson MJ, Waite JH. Ferric ion complexes of a Dopa-containing adhesive protein from *Mytilus edulis*. *Inorg. Chem.* 1996; 35:7572–77.
40. Sever MJ, Weissner JT, Monahan J, Srinivasan S, Wilker JJ. Metal-mediated cross-linking in the generation of a marine-mussel adhesive. *Angew. Chem.* 2004; 43:448–50. [PubMed: 14735531]
41. Anderson TH, Yu J, Estrada AY, Hammer MU, Waite JH, Israelachvili JN. The contribution of Dopa to substrate-peptide adhesion and internal cohesion of mussel-inspired synthetic peptide films. *Adv. Funct. Mater.* 2010; 20:4196–205. [PubMed: 21603098]
42. Zhao H, Sun CJ, Stewart RJ, Waite JH. Cement proteins of the tube building polychaete *Phragmatopoma californica*. *J. Biol. Chem.* 2005; 280:42938–44. [PubMed: 16227622]
43. Shao H, Stewart RJ. Biomimetic underwater adhesives with environmentally triggered setting mechanisms. *Adv. Mater.* 2010; 22:729–33. [PubMed: 20217779]
44. Hwang DS, Zeng H, Srivastava A, Krogstad DV, Tirrell M, et al. Viscosity and interfacial properties in a mussel-inspired coacervate. *Soft Matter*. 2010; 6:3232–36. [PubMed: 21544267]
45. Lim S, Choi YS, Kang DG, Song YH, Cha HJ. The adhesive properties of coacervated recombinant hybrid mussel adhesive proteins. *Biomaterials*. 2010; 31:3715–22. [PubMed: 20144475]
46. Holten-Andersen N, Waite JH. Mussel-designed protective coatings for compliant substrates. *J. Dent. Res.* 2008; 87:701–9. [PubMed: 18650539]
47. Holten-Andersen N, Zhao H, Waite JH. Stiff coatings on compliant biofibers: the cuticle of *Mytilus californianus* byssal threads. *Biochemistry*. 2009; 48:2752–59. [PubMed: 19220048]
48. Holten-Andersen N, Fantner GE, Hohlbauch S, Waite JH, Zok FW. Protective coatings on extensible biofibers. *Nat. Mater.* 2007; 6:669–72. [PubMed: 17618290] The first application of nanoindentation for hardness and stiffness measurements in hydrated byssal coatings.
49. Vitellaro Zuccarello L. Ultrastructural and cytochemical study on the enzyme gland of the foot of a mollusc. *Tissue Cell*. 1981; 13:701–13. [PubMed: 6800062] The only known ultrastructural study of the formation of the byssal cuticle.
50. Sun CJ, Waite JH. Mapping chemical gradients within and along a fibrous structural tissue: mussel byssal threads. *J. Biol. Chem.* 2005; 280:39332–36. [PubMed: 16166079]
51. Holten-Andersen N, Toprak M, Stucky GD, Zok FW, Waite JH. Metals and the integrity of a biological coating: the cuticle of mussel byssus. *Langmuir*. 2009; 25:3323–26. [PubMed: 18847291]
52. Waite JH. Evidence for a repeated DOPA- and hydroxyproline containing decapeptide in the adhesive protein of the mussel *Mytilus edulis*. *J. Biol. Chem.* 1983; 258:2911–15. [PubMed: 6298211]
53. Taylor SW, Waite JH, Ross MM, Shabanowitz J, Hunt DF. *trans*-2,3-*cis*-3,4-Dihydroxyproline in the tandemly repeated consensus decapeptides of an adhesive protein from *Mytilus edulis*. *J. Am. Chem. Soc.* 1994; 116:10803–4.
54. Haemers, S. *The Adhesive of the Blue Mussel: Controlling Cross-Linking*. DUP Sci.; Delft: 2003.

55. Karpishin TB, Gebhard MS, Solomon EI, Raymond KN. Spectroscopic studies of the electronic structure of iron (III) triscatecholates. *J. Am. Chem. Soc.* 1991; 113:2977–84. Classic analysis and modeling of charge transfer in triscatecholate Fe³⁺ complexes.
56. Zeng H, Hwang DS, Israelachvili JN, Waite JH. Strong reversible Fe³⁺ mediated bridging between Dopa-containing protein films in water. *Proc. Natl. Acad. Sci. USA.* 2010; 107:12850–53. [PubMed: 20615994] First nanomechanical test of cross-links based on Fe³⁺ coordination by a Dopa-containing protein.
57. McDowell LM, Burzio LA, Waite JH, Schaefer J. REDOR detection of cross-links formed in mussel byssus under high flow stress. *J. Biol. Chem.* 1999; 274:20293–95. [PubMed: 10400649]
58. Sagert, J.; Sun, C.J.; Waite, JH. Chemical subtleties of mussel and polychaete holdfasts. In: Smith, AM.; Callow, JA., editors. *Biological Adhesives*. Springer-Verlag; Berlin: 2006. p. 257–78.
59. Yamamoto H. Adhesive studies of synthetic polypeptides: a model for marine adhesive proteins. *J. Adhes. Sci. Technol.* 1987; 1:177–83.
60. Yamamoto H, Yamauchi S, Ohara S. Synthesis and adhesive studies of marine adhesive proteins of the Chilean mussel *Aulacomya ater*. *Biomimetics.* 1992; 1:219–38.
61. Yamamoto H, Ohkawa K. Synthesis of adhesive protein from the vitellaria of the liver fluke *Fasciola hepatica*. *Amino Acids.* 1993; 5:71–75.
62. Tatehata H, Mochizuki A, Kawashima T, Yamashita S, Yamamoto H. Model polypeptide of mussel adhesive protein. I. Synthesis and adhesive studies of sequential polypeptides (X-Tyr-Lys)_n and (Y-Lys)_n. *J. Appl. Polym. Sci.* 2000; 76:929–37.
63. Yu M, Deming TJ. Synthetic polypeptide mimics of marine adhesives. *Macromolecules.* 1998; 31:4739–45. [PubMed: 9680407]
64. Yu M, Hwang J, Deming TJ. Role of L-3,4-dihydroxyphenylalanine in mussel adhesive proteins. *J. Am. Chem. Soc.* 1999; 121:5825–26.
65. Yin M, Yuan Y, Liu C, Wang J. Development of mussel adhesive polypeptide mimics coating for in-situ inducing re-endothelialization of intravascular stent devices. *Biomaterials.* 2009; 30:2764–73. [PubMed: 19223071]
66. Maugh, KJ.; Anderson, DM.; Strausberg, R.; Strausberg, SL.; McCandliss, R., et al. U.S. Patent. No. 87-US3048. 1988.
67. Strausberg RL, Anderson DM, Filpula D, Finkelman M, Link R, et al. Development of a microbial system for production of mussel adhesive protein. *ACS Symp.* 1989; 385:453–64.
68. Filpula DR, Lee SM, Link RP, Strausberg SL, Strausberg RL. Structural and functional repetition in a marine mussel adhesive protein. *Biotechnol. Prog.* 1990; 6:171–77. [PubMed: 1367451]
69. Strausberg RL, Link RP. Protein-based medical adhesives. *Trends Biotechnol.* 1990; 8:53–57. [PubMed: 1366498]
70. Deming TJ. Mussel byssus and biomolecular materials. *Curr. Opin. Chem. Biol.* 1999; 3:100–5. [PubMed: 10021411]
71. Cha HJ, Hwang DS, Lim S. Development of bioadhesives from marine mussels. *Biotechnol. J.* 2008; 3:631–38. [PubMed: 18293310]
72. Lee BP, Dalsin JL, Messersmith PB. Synthesis and gelation of DOPA-modified poly(ethylene glycol) hydrogels. *Biomacromolecules.* 2002; 3:1038–47. [PubMed: 12217051]
73. Brubaker CE, Kissler H, Wang L-J, Kaufman DB, Messersmith PB. Biological performance of mussel-inspired adhesive in extrahepatic islet transplantation. *Biomaterials.* 2010; 31:420–27. [PubMed: 19811819]
74. Lee BP, Huang K, Nunalee FN, Shull KR, Messersmith PB. Synthesis of 3,4-dihydroxyphenylalanine (DOPA) containing monomers and their copolymerization with PEG-diacrylate to form hydrogels. *J. Biomater. Sci. Polym. Ed.* 2004; 15:449–64. [PubMed: 15212328]
75. Glass P, Chung H, Washburn NR, Sitti M. Enhanced reversible adhesion of dopamine methacrylamide-coated elastomer microfibrillar structures under wet conditions. *Langmuir.* 2009; 25:6607–12. [PubMed: 19456091]
76. Lee H, Lee BP, Messersmith PB. A reversible wet/dry adhesive inspired by mussels and geckos. *Nature.* 2007; 448:338–41. [PubMed: 17637666] Amusing and inspiring biomimetic fusion of mussel and gecko adhesion.

77. Shao H, Bachus KN, Stewart RJ. A water-borne adhesive modeled after the sandcastle glue of *P. californica*. *Macromol. Biosci.* 2009; 9:464–71. [PubMed: 19040222]
78. Daly WH, Moulay S. Synthesis of poly(vinylcatechols). *J. Polym. Sci.* 1986; 74:227–42.
79. Yang Z, Pelton R. The synthesis of poly(3,4-dihydroxystyrene) and poly[(sodium 4-styrenesulfonate)-*co*(3,4-dihydroxystyrene)]. *Macromol. Rapid Commun.* 1998; 19:241–46.
80. Westwood G, Horton TN, Wilker JJ. Simplified polymer mimics of cross-linking adhesive proteins. *Macromolecules.* 2007; 40:3960–64.
81. Lee, BP. U.S. Patent. No. 7,622,533. 2009.
82. Charlot A, Sciannamea V, Lenoir S, Faure E, Jerome R, et al. All-in-one strategy for the fabrication of antimicrobial biomimetic films on stainless steel. *J. Mater. Chem.* 2009; 19:4117–25.
83. Pan X-D, Qina Z, Yana Y-Y, Sadhukhana P. Elastomers with chain-end mussel-mimetic modification for nanocomposites: strong modifications to reinforcement and viscoelastic properties. *Polymer.* 2010; 51:3453–61.
84. Lee, B.; Dalsin, JL.; Messersmith, PB. Biomimetic adhesive polymers based on mussel adhesive proteins. In: Smith, AM.; Callow, JA., editors. *Biological Adhesives*. Springer-Verlag; Berlin: 2006. p. 257-78.
85. Catron N, Lee H, Messersmith PB. Enhancement of poly(ethylene glycol) mucoadsorption by biomimetic end group functionalization. *Biointerphases.* 2006; 1:134–41. [PubMed: 20408626]
86. Mowery CL, Crosby AJ, Ahn D, Shull KR. Adhesion of thermally reversible gels to solid surfaces. *Langmuir.* 1997; 13:6101–7.
87. Flanigan CM, Crosby AJ, Shull KR. Structural development and adhesion of acrylic ABA triblock copolymer gels. *Macromolecules.* 1999; 32:7251–62.
88. Flanigan CM, Shull KR. Adhesive and elastic properties of thin gel layers. *Langmuir.* 1999; 15:4966–74.
89. Deruelle M, Leger L, Tirrell M. Adhesion at the solid-elastomer interface: influence of the interfacial chains. *Macromolecules.* 1995; 28:7419–28.
90. Johnson KL, Kendall K, Roberts AD. Surface energy and the contact of elastic solids. *Proc. R. Soc. Lond.* 1971; 324:301–13.
91. Burke SA, Ritter-Jones M, Lee BP, Messersmith PB. Thermal gelation and tissue adhesion of biomimetic hydrogels. *Biomed. Mater.* 2007; 2:203–10. [PubMed: 18458476]
92. Ninan L, Monahan J, Stroshine RL, Wilker JJ, Shi R. Adhesive strength of marine mussel extracts on porcine skin. *Biomaterials.* 2003; 24:4091–99. [PubMed: 12834605]
93. da Silva LFM, Rodrigues TNSS, Figueiredo MAV, de Moura MFSF, Chousal JAG. Effect of adhesive type and thickness on the lap shear strength. *J. Adhes.* 2006; 82:1091–115.
94. Lee BP, Chao C-Y, Nunalee FN, Motan E, Shull KR, Messersmith PB. Rapid gel formation and adhesion in photocurable and biodegradable block copolymers with high DOPA content. *Macromolecules.* 2006; 39:1740–48.
95. Guvendiren M, Brass DA, Messersmith PB, Shull KR. Adhesion of DOPA-functionalized model membranes to hard and soft surfaces. *J. Adhes.* 2009; 86:631–45. [PubMed: 21461121]
96. Messersmith, PB.; Lee, BP.; Dalsin, JL.; Burke, SA. U.S. Patent. No. 20,080,247,984. 2008.
97. Dalsin, JL.; Lee, BP.; Vollenweider, L.; Silvary, S.; Murphy, JL., et al. U.S. Patent. No. 20,100,113,828. 2010.
98. Bilic G, Brubaker C, Messersmith PB, Mallik AS, Quinn TM, et al. Injectable candidate sealants for fetal membrane repair: bonding and toxicity in vitro. *Am. J. Obstet. Gynecol.* 2010; 202:85.e1–9. [PubMed: 20096254]
99. Winslow BD, Shao H, Stewart RJ, Tresco PA. Biocompatibility of adhesive complex coacervates modeled after the sandcastle glue of *Phragmatopoma californica* for craniofacial reconstruction. *Biomaterials.* 2010; 31:9373–81. [PubMed: 20950851]
100. Dalsin JL, Messersmith P. Bioinspired antifouling polymers. *Mater. Today.* 2005; 8:38–46.
101. Lee H, Dellatore SM, Miller WM, Messersmith PB. Mussel-inspired surface chemistry for multifunctional coatings. *Science.* 2007; 318:426–30. [PubMed: 17947576] Catechol chemistry simply reformulated as a general platform for surface modification.

102. Ko R, Cadieux PA, Dalsin JL, Lee BP, Elwood CN, Razvi H. Novel uropathogen-resistant coatings inspired by marine mussels. *J. Endourol.* 2008; 22:1153–60. [PubMed: 18484883]
103. Dong, B.; Xu, F.; Lyman, A.; Cadieux, P.; Vollenweider, L., et al. Proc. Biointerface 2009. San Mateo, CA: 2009. Inhibition of bacterial attachment by mussel-inspired coatings on urinary stents and catheter materials.
104. Pechey A, Elwood CN, Wignall GR, Dalsin JL, Lee BP, et al. Anti-adhesive coating and clearance of device associated uropathogenic *Escherichia coli* cystitis. *J. Urol.* 2009; 182:1628–36. [PubMed: 19683735]
105. Gunawan R, King J, Lee BP, Messersmith PB, Miller W. Surface presentation of bioactive ligands in a non-adhesive background using DOPA-tethered biotinylated poly(ethylene glycol). *Langmuir.* 2007; 23:10635–43. [PubMed: 17803326]
106. Statz AR, Barron AE, Messersmith PB. Protein, cell and bacterial fouling resistance of polypeptoid-modified surfaces: effect of side-chain chemistry. *Soft Matter.* 2008; 4:131–39. [PubMed: 21472038]
107. Statz AR, Kuang J, Ren C, Barron AE, Szeleifer I, Messersmith PB. Experimental and theoretical investigation of chain length and surface coverage on fouling of surface grafted polypeptoids. *Biointerphases.* 2009; 4:FA22–32. [PubMed: 20300542]
108. Statz AR, Meagher RJ, Barron AE, Messersmith PB. New peptidomimetic polymers for antifouling surfaces. *J. Am. Chem. Soc.* 2005; 127:7972–73. [PubMed: 15926795]
109. Brault ND, Gao C, Xue H, Piliarik M, Homola J, et al. Ultra-low fouling and functionalizable zwitterionic coatings grafted onto SiO₂ via a biomimetic adhesive group for sensing and detection in complex media. *Biosens. Bioelectron.* 2010; 25:2276–82. [PubMed: 20359880]
110. Gao C, Li G, Xue H, Yang W, Zhang F, Jiang S. Functionalizable and ultra-low fouling zwitterionic surfaces via adhesive mussel mimetic linkages. *Biomaterials.* 2010; 31:1486–92. [PubMed: 19962753]
111. Chua P-H, Neoh K-G, Kang E-T, Wang W. Surface functionalization of titanium with hyaluronic acid/chitosan polyelectrolyte multilayers and RGD for promoting osteoblast functions and inhibiting bacterial adhesion. *Biomaterials.* 2008; 29:1412–21. [PubMed: 18190959]
112. Shi Z, Neoh KG, Kang E-T, Poh C, Wang W. Titanium with surface-grafted dextran and immobilized bone morphogenetic protein-2 for inhibition of bacterial adhesion and enhancement of osteoblast functions. *Tissue Eng. A.* 2009; 15:417–26.
113. Hu X, Neoh K-G, Shi Z, Kang E-T, Poh C, Wang W. An in vitro assessment of titanium functionalized with polysaccharides conjugated with vascular endothelial growth factor for enhanced osseointegration and inhibition of bacterial adhesion. *Biomaterials.* 2010; 31:8854–63. [PubMed: 20800276]
114. Paunesku T, Rajh T, Wiederrecht G, Maser J, Vogt S, et al. Biology of TiO₂-oligonucleotide nanocomposites. *Nat. Mater.* 2003; 2:343–46. [PubMed: 12692534]
115. Xu C, Xu K, Gu H, Zheng R, Liu H, et al. Dopamine as a robust anchor to immobilize functional molecules on the iron oxide shell of magnetic nanoparticles. *J. Am. Chem. Soc.* 2004; 126:9938–39. [PubMed: 15303865]
116. Lee Y, Lee H, Kim YB, Kim J, Hyeon T, et al. Bioinspired surface immobilization of hyaluronic acid on monodisperse magnetite nanocrystals for targeted cancer imaging. *Adv. Mater.* 2008; 20:4154–57. [PubMed: 19606262]
117. Sun I-C, Eun D-K, Na JH, Lee S, Kim I-J, et al. Heparin-coated gold nanoparticles for liver-specific CT imaging. *Chem. Eur. J.* 2009; 15:13341–47.
118. Yang C, Yang Z, Gu H, Chang CK, Gao P, Xu B. Facet-selective 2D self-assembly of TiO₂ nanoleaves via supramolecular interactions. *Chem. Mater.* 2008; 20:7514–20.
119. Amstad E, Gillich T, Bilecka I, Textor M, Reimhult E. Ultrastable iron oxide nanoparticle colloidal suspensions using dispersants with catechol-derived anchor groups. *Nano Lett.* 2009; 9:4042–48. [PubMed: 19835370]
120. Araujo PZ, Morando PJ, Blesa MA. Interaction of catechol and gallic acid with titanium dioxide in aqueous suspensions. 1. Equilibrium studies. *Langmuir.* 2005; 21:3470–74. [PubMed: 15807589]

121. Sun CJ, Srivastava A, Reifert JR, Waite JH. Halogenated DOPA in a marine adhesive protein. *J. Adhes.* 2009; 85:126–38. [PubMed: 20126508]

Work of adhesion: W_A^{12} is the work done on the system when two condensed phases 1 and 2 ($1 \neq 2$) that form an interface of unit area are separated reversibly to form unit surface areas of each of the phases

Byssus: an extraorganismic proteinaceous holdfast structure produced by many bivalve mollusks for opportunistic adhesion to hard surfaces

mfp: mussel foot protein

Dopa: 3,4-dihydroxyphenyl-L-alanine

MALDI-TOF: matrix-assisted laser desorption ionization time of flight

Redox balance: the state of maintaining a specific stoichiometry between oxidation and reduction reactions

Raman microscopy: a type of confocal microscopy with micrometer resolution based on Raman scattering of monochromatic light

Surface forces apparatus (SFA): a versatile instrument with angstrom and nanonewton resolution for measuring surface forces between the surfaces of condensed phases

Chelation: multidentate coordination of a metal ion by a ligand. Dopa chelation of iron is bidentate; i.e., both hydroxyl groups bind iron by replacing hydroxyl groups in iron hydroxide

Catechol: abenzene ring with two *ortho*-placed hydroxyl groups. Dopa is a catechol

PEG: poly(ethylene glycol)

DMAm: Dopamine methacrylamide

MEA: 2-methoxyethyl acrylate

p(DMAm-co-MEA): poly(Dopamine-methacrylamide-co-2-methoxyethyl acrylate)

p(DMAm-co-mPEG-MA): poly[Dopamine-methacrylamide-co-poly(ethylene glycol)-methylether methacrylate]

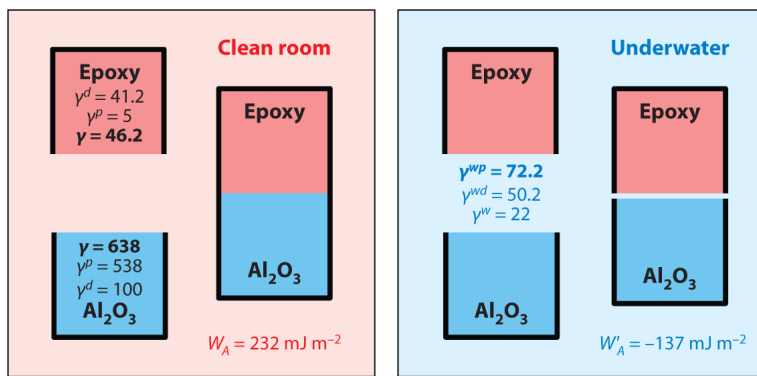
Grafting to/from: refers to the polymer modification of surfaces in which a fully formed polymer is either adsorbed to a surface (“to”) or polymerized from anchoring points on the surface (“from”) by surface-initiated polymerization

SUMMARY POINTS

1. Practical underwater adhesives must have the ability to remove weak boundary layers and compete with surface hydration; to spread spontaneously on surfaces; to be deliverable as dense, phase-separated fluids; to undergo energetic interfacial interactions with the substratum; and to become cross-linked or cured for cohesive strength. Mussel adhesives appear to satisfy these requirements.
2. Despite the presence of moisture and fouling biofilms, mussel adhesive plaques secure intimate contact with at least patches of bare surface. Dopa provides bidentate or covalent interfacial interactions on most surfaces. Protein coacervation also offers advantages such as spontaneous spreading on most surfaces and reduced diffusive loss of adhesive proteins by a phase-separation process that concentrates proteins at up to 1 g cc^{-1} .
3. Mussel foot proteins gain cohesiveness through three known mechanisms: intrinsic protein-protein binding, metal chelation, and covalent coupling. Dopa is crucial for at least two of these.
4. At present, Dopa chemistry is the main focus of mussel-inspired engineering of synthetic adhesives, sealants, coatings, and polymer anchors. Coacervation of synthetic polyelectrolytes is also beginning to show promise.
5. The need for investigating the wet adhesion of mussels and other sessile organisms hardly ends with the discovery of Dopa. Dopa is a highly reactive functionality posing serious drawbacks when control of reactivity is critical to the application. Mussels have consummate talents in directing this reactivity in many different directions.

FUTURE ISSUES

1. Can the susceptibility of Dopa, or catecholic side chains generally, to oxidation be precisely controlled in polymers? Put another way, can researchers engineer side chains that possess the facile bidentate surface binding of Dopa without the tendency to oxidize?
2. Some of the intrinsic protein-protein interactions between different mussel foot proteins are very strong. What is the molecular basis for these interactions?
3. How important is covalent cross-linking for adhesive performance? In mussels, is cross-linking adaptive, or is it a collateral damage that accompanies oxidation during aging?
4. Dopa functionalities of proteins and other polymers mediate adhesion to a variety of surface chemistries that have little to nothing in common with one another. Is there a single fundamental reason for the stickiness of Dopa and related catechols?



$$W_A = 2\sqrt{\gamma_1^d \gamma_2^d} + 2\sqrt{\gamma_1^p \gamma_2^p}$$

$$W_A = 2\left\{ \begin{matrix} \sqrt{\gamma_1^d \gamma_w^d} & - & \sqrt{\gamma_1^p \gamma_w^p} & - & \sqrt{\gamma_2^d \gamma_w^d} & - & \sqrt{\gamma_2^p \gamma_w^p} & + & \sqrt{\gamma_1^d \gamma_2^d} & + & \sqrt{\gamma_1^p \gamma_2^p} \end{matrix} \right\}$$

-30
-16
-47
-164
+64
+52

Figure 1. The influence of water on the work of adhesion (W_A) between an epoxy adhesive and an aluminum surface. W_A is derived from the summation of surface energy products due to dispersion interactions ($\gamma_1^d \gamma_2^d$) and those due to polar interactions ($\gamma_1^p \gamma_2^p$) under clean-room (*left*) and wet (*right*) conditions. From data in Pocius (5).

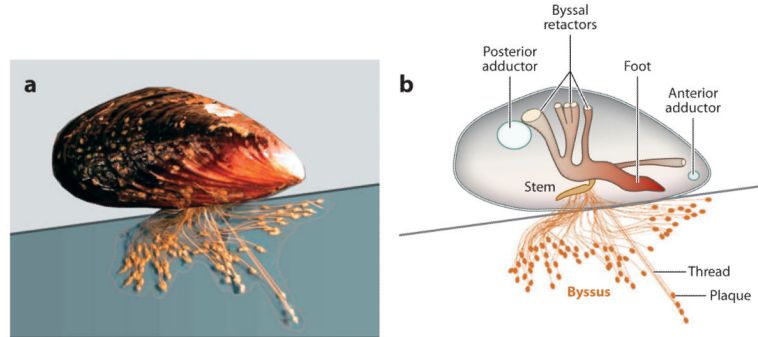


Figure 2. Adhesion in the marine mussel *Mytilus californianus*. (a) Adult mussel (5 cm length) displaying an extensive byssus attached to a mica surface. (b) Schematic mussel on a half-shell. Each byssus is a bundle of threads tipped with adhesive plaques. The threads are joined at the stem, which inserts into the base of the foot. Byssal tension is controlled by 12 byssal retractor muscles, 6 per valve. The two adductor muscles open and close the valves.

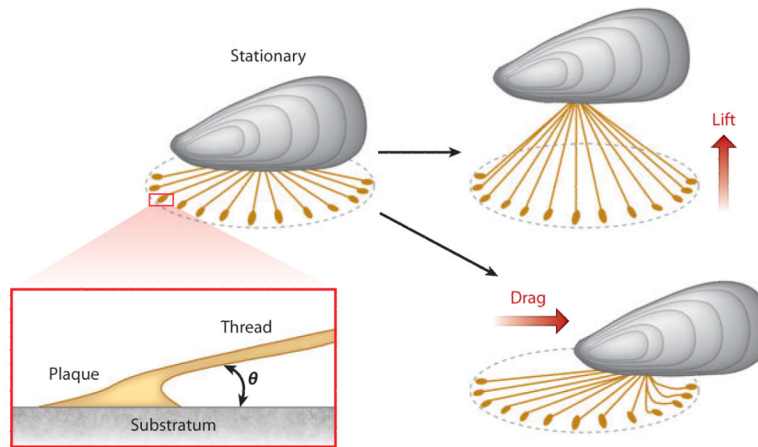


Figure 3. Mussels in flow experience a combination of lift and drag. (*Left*) Shown is a mussel in stationary water with an idealized byssus in which radial, equidistant threads of the same length form a small angle θ with the surface. (*Right*) Lift is force applied normal to the surface, whereas drag is force applied parallel to the surface. The location of the thread-to-plaque connection is biased toward the plaque's proximal edge.

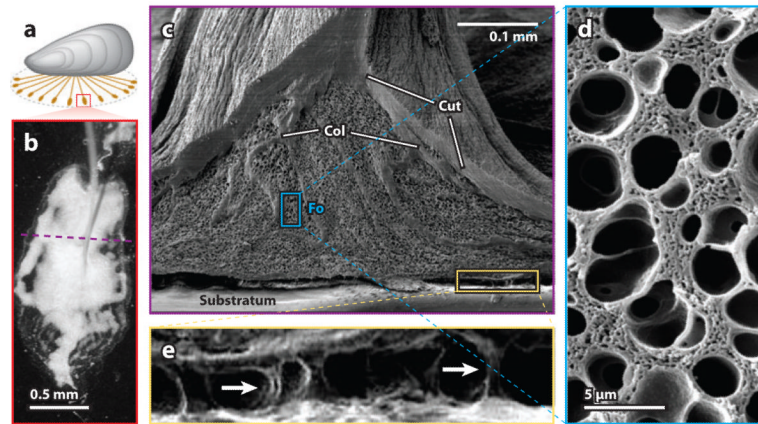


Figure 4. The ultrastructure of a byssal adhesive plaque. (a) A byssated mussel showing the orientation of the sampled adhesive plaque (red). (b) Microscopic, reflected light image of a single attached plaque of *Mytilus californianus*. The underlying foam-like structure causes the light-scattering effect (white). The purple dashed line indicates the position of the freeze fracture. (c) Scanning electron microscope view of a freeze-fractured plaque illustrating the cuticle (Cut), the collagen fibers (Col) from the core, and the foam (Fo). (d) An enlargement of the foam-like structure shown in the blue boxed region in panel c. (e) The interfacial region between the plaque and the substratum shown in the yellow boxed region in panel c. A number of pillars (arrows) remain intact despite partial plaque delamination due to drying.

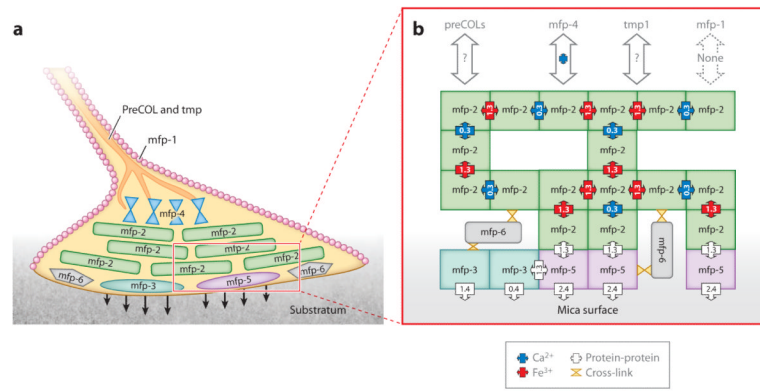


Figure 6.

Schematic view of mussel foot proteins (mfps) in a byssal plaque of *Mytilus* showing the approximate location of each of the major proteins. (a) Mfp-3 variants and mfp-5 are thought to be the adhesives (arrows). Mfp-2 makes up the core of each plaque. The entire plaque is coated by a cuticle made of mfp-1 and Fe³⁺. Mfp-4 may mediate links between the prepolymerized collagen (preCOL) fibers descending from the thread core to other proteins in the plaque. The red boxed region is enlarged in panel b. (b) Schematic view of all known mfp interactions as determined by the surface forces apparatus (SFA). Mfp-3 and mfp-5 are responsible for the primary adhesive interactions with the surface. Only mfp-5 interacts with mfp-3, and only mfp-2 interacts with mfp-5. Interactions between mfp-2s are entirely Ca²⁺ (blue) and Fe³⁺ (red) mediated. A Ca²⁺-mediated interaction between mfp-2 and mfp-4 also exists. Work-of-adhesion values for mfp-3 correspond to reducing (1.4 mJ m⁻²) and oxidizing (0.4 mJ m⁻²) conditions in the SFA. Interactions denoted by a question mark remain to be determined. Tmp denotes thread matrix protein. Adapted from research originally published in Reference 24, copyright © the American Society for Biochemistry and Molecular Biology.

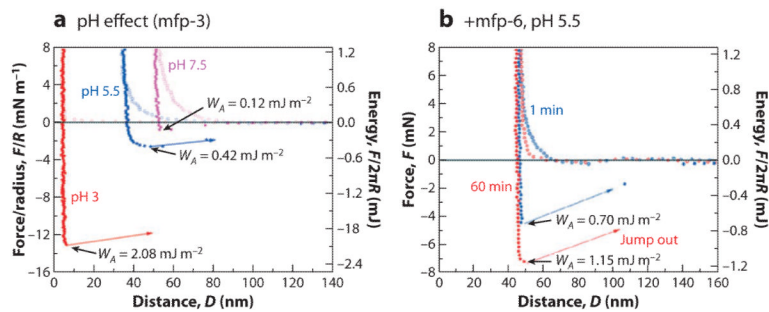


Figure 7.

Adhesion loss and recovery in mfp-3 films on mica as measured in the surface forces apparatus.

(a) Symmetric mfp-3 films show their greatest interaction at pH 3 and diminish immediately with increasing pH. (b) Addition of 100 pmol of mfp-6 to the gap solution recovers nearly 200% adhesion after 1 min and 300% after a 60-min contact. Data from Yu et al. (31).

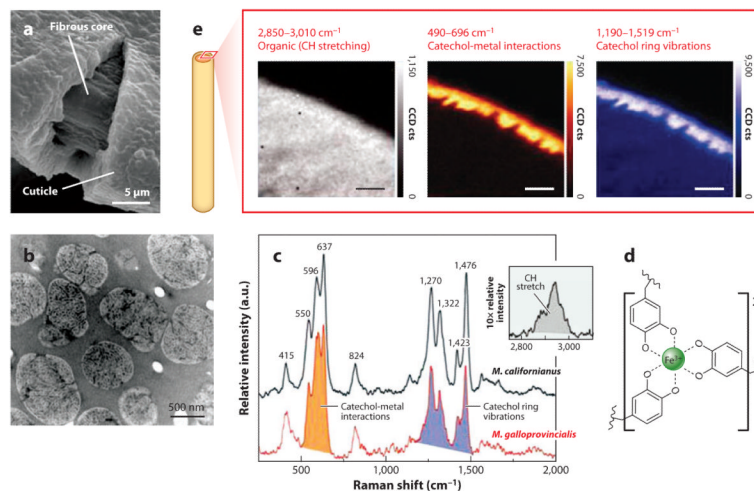


Figure 8.

The cuticle of *Mytilus* byssus. (a) Scanning electron micrograph of a cracked cuticle showing the thickness relative to the underlying fibers. This thread was stretched to 120% its initial length. (b) Transmission electron micrograph of a 1- μm -thick section of the cuticle in *Mytilus galloprovincialis*. There is a continuous homogeneous matrix filled with marbled inclusions. (c) Resonance Raman spectra taken of cuticular thin sections of *Mytilus californianus* (black line) and *M. galloprovincialis* (red line) using a 785-nm laser. (d) A tris-Fe(III)-Dopa complex. (e) Confocal Raman micrographs of byssal cuticle imaged at the C-H stretching shift (left), at the catechol-O-Fe(III) shift (center), and at the Dopa ring vibrations (right). Adapted from research originally published in Reference 38, copyright © AAAS.

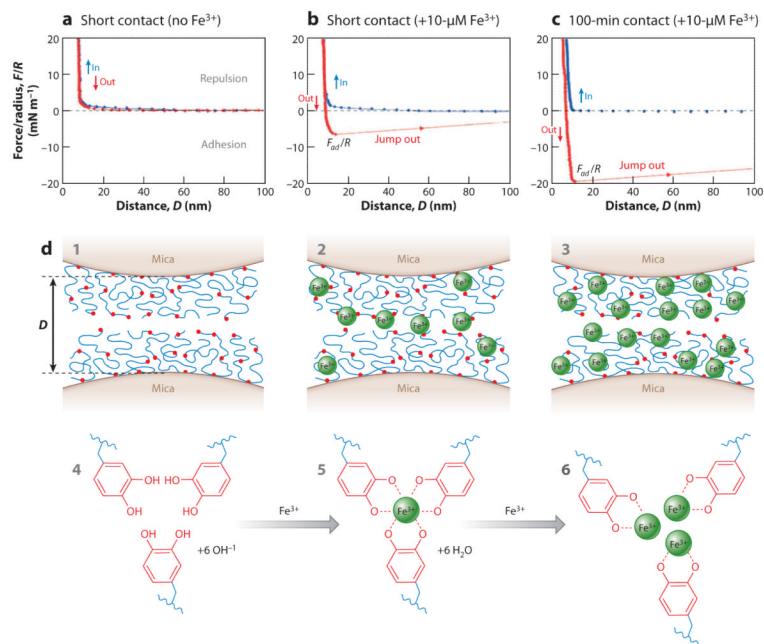
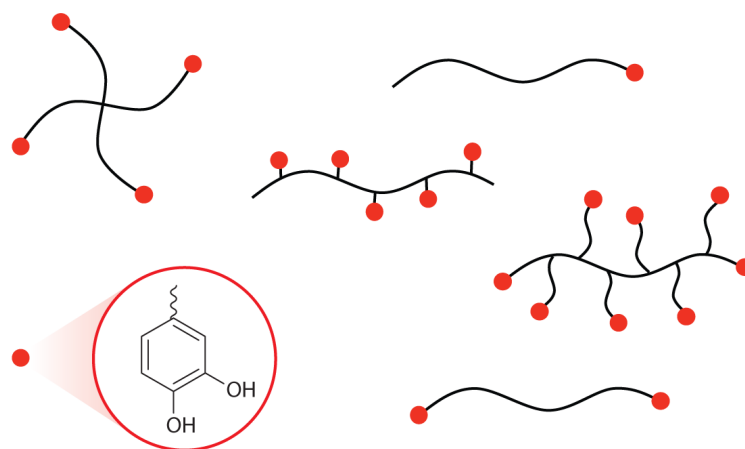


Figure 9.

Fe^{3+} bridging of symmetric mfp-1 films on mica, as measured by the surface forces apparatus. (a) Without Fe^{3+} there is no interaction after contact. (b) Addition of $10\text{-}\mu\text{M}$ Fe^{3+} results in an immediate interaction evident by the jump-out peaking at 7 mN m^{-1} . (c) A 100-min contact increases the interaction to 20 mN m^{-1} . (d) Schematic showing two opposed symmetric mfp-1 films on mica (1) without Fe^{3+} , (2) with $10\text{-}\mu\text{M}$ Fe^{3+} , and (3) with $100\text{-}\mu\text{M}$ Fe^{3+} . Also shown are the suggested chemical interactions between Dopa and Fe^{3+} : (4) no Fe^{3+} , (5) tris-Dopa- Fe^{3+} complexes, and (6) mono-Dopa- Fe^{3+} complexes. This research was originally published in Reference 56, copyright © National Academy of Sciences.

**Figure 10.**

Schematic illustration of mussel adhesive protein mimetic polymer systems. The red circles represent Dopa or a catechol mimic of Dopa covalently coupled to polymer chain ends or as side chains of polymerizable catechol monomers. The polymer backbone is linear or branched and is conceivably of any composition but most commonly consists of polypeptides, poly(ethylene glycol), poly(acrylate/methacrylate), or poly(acrylamide/methacrylamide).

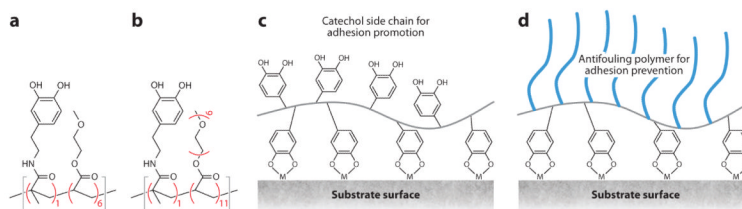


Figure 11. Chemical structures of catechol-functionalized polymers. (a) poly(Dopamine-methacrylamide-*co*-2-methoxyethyl acrylate) [p(DMAm-*co*-MEA)] and (b) poly[Dopamine-methacrylamide-*co*-poly(ethylene glycol)-methylether methacrylate] [p(DMAm-*co*-mPEG-MA)]. Schematic representation of these polymers functioning as (c) adhesive or (d) antifouling coatings. Adapted from Reference 81 with permission.

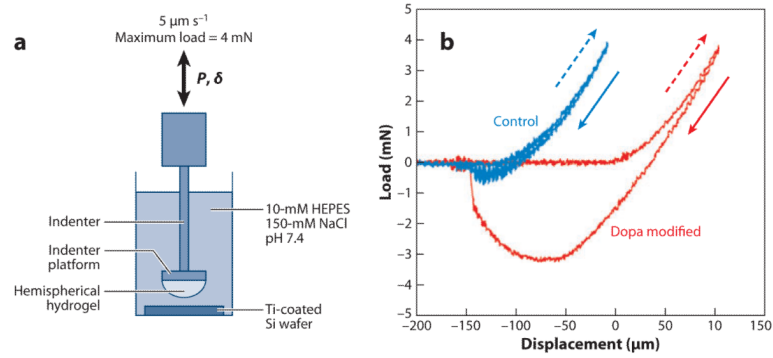


Figure 12.

(a) Contact mechanics experimental design and (b) load-versus-displacement curves of control (*blue*) and Dopa-modified (*red*) gels contacting a Ti-coated silicon wafer submerged in aqueous buffer. Dashed arrows indicate the advancing (indentation) portion of the curve, whereas solid arrows indicate the receding (pull-off) portion of the contact curve. Adapted from Reference 94 with permission.

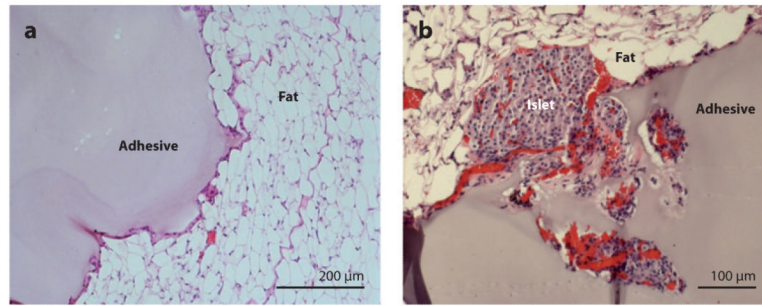


Figure 13. Histological results from implantation of PEG-catechol hydrogel into mice. (a) Hematoxylin-eosin-stained tissue section showing the adhesive in contact with fat tissue after 6 weeks of implantation. Note the close apposition of the adhesive to the fat tissue and limited inflammatory cell infiltration. (b) Hematoxylin-eosin-stained tissue section showing a site of mouse islet transplantation using the PEG-catechol gel as a sealant to immobilize islets onto the fat tissue surface. The graft was removed on day 100 following transplantation. Revascularization of the islet is apparent from the presence of several blood vessels containing erythrocytes (*red*). Adapted from Reference 73 with permission.

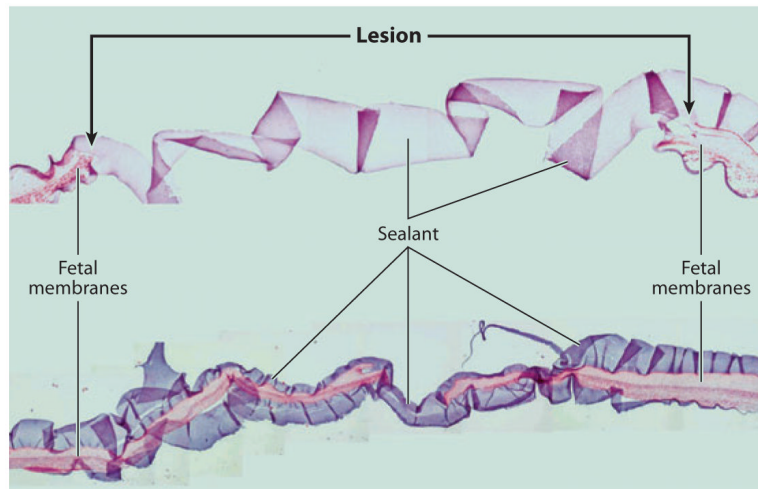


Figure 14.

Ex vivo sealing of fetal membrane defects with PEG-catechol adhesive. Through-thickness puncture wounds (*sealant lines*) were created on fresh fetal membranes with an ~3.5-mm trocar, and approximately 0.5 ml of adhesive was applied over the defect. The images represent a collage of a hematoxylin- and eosin-stained cross section through the defect and the PEG-catechol adhesive. The hydrogel appears as a ribbon-like structure that bridges the puncture edges. The bottom image shows a cross section of the same lesion at a narrow location. Adapted from Reference 98 with permission.

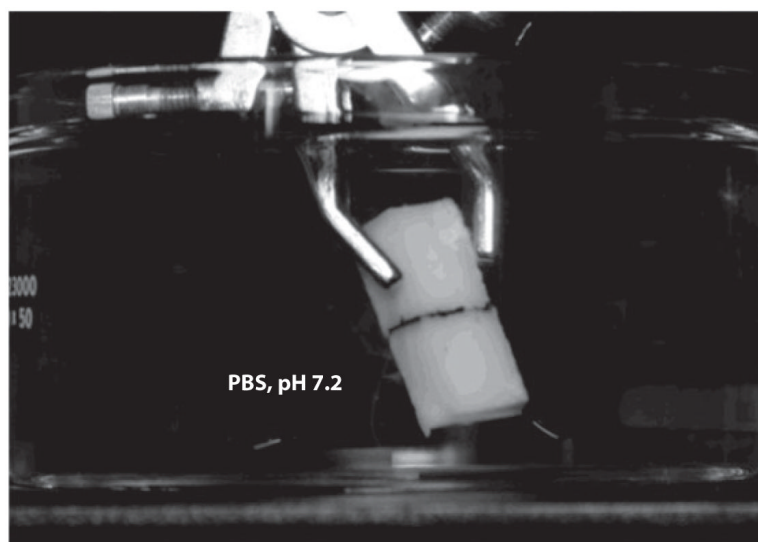


Figure 15. Photograph of bone slabs glued together with a complex coacervate formulation based on a synthetic polymer adhesive modeled after sandcastle worm cement. PBS denotes phosphate-buffered saline. From Reference 77 with permission. Copyright © 2009 Wiley-VCH.

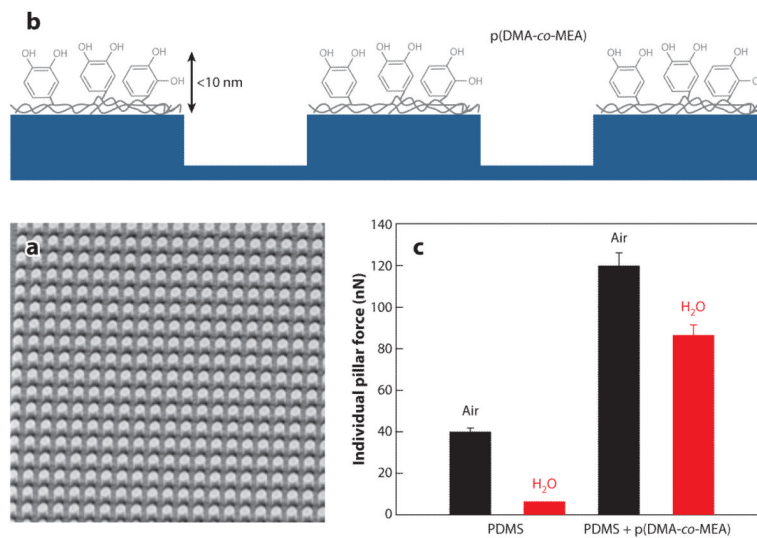


Figure 16.

Gecko- and mussel-inspired wet/dry adhesive. A thin silicone elastomer film containing pillar projections (*a*) was fabricated by nanolithography and then coated with a thin film of mussel adhesive protein mimetic polymer (*b*). Adhesion force per pillar in untreated and mussel mimetic polymer-coated polydimethylsiloxane (PDMS) is compared in panel *c*. p(DMA-co-MEA) denotes poly(Dopamine-methacrylamide-co-2-methoxyethyl acrylate). Adapted from Reference 76 with permission.

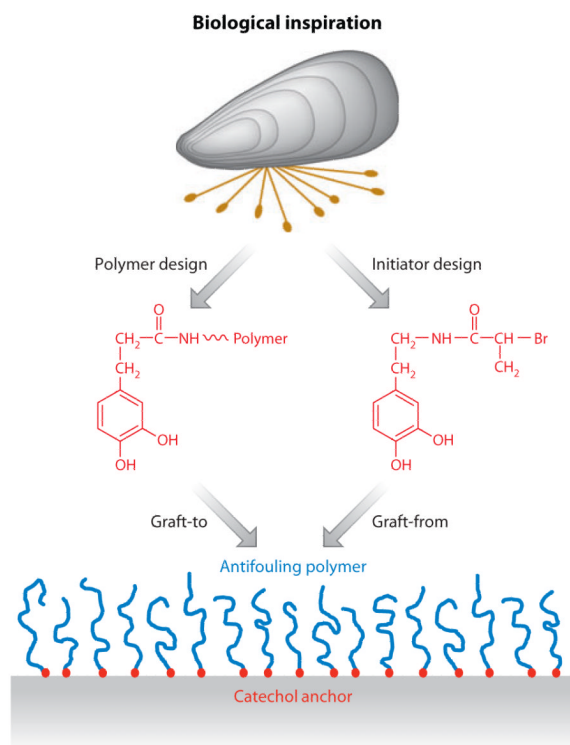


Figure 17. Schematic illustration of a biologically inspired strategy for grafting antifouling polymers onto surfaces. The anchors exploit the adhesive nature of catechols such as Dopa or Dopa peptides inspired by mussel adhesive proteins. Catechol anchors may be chemically coupled to an antifouling polymer and adsorbed onto a surface (a graft-to approach) or to an initiator that is used for surface-initiated polymerization (a graft-from approach).

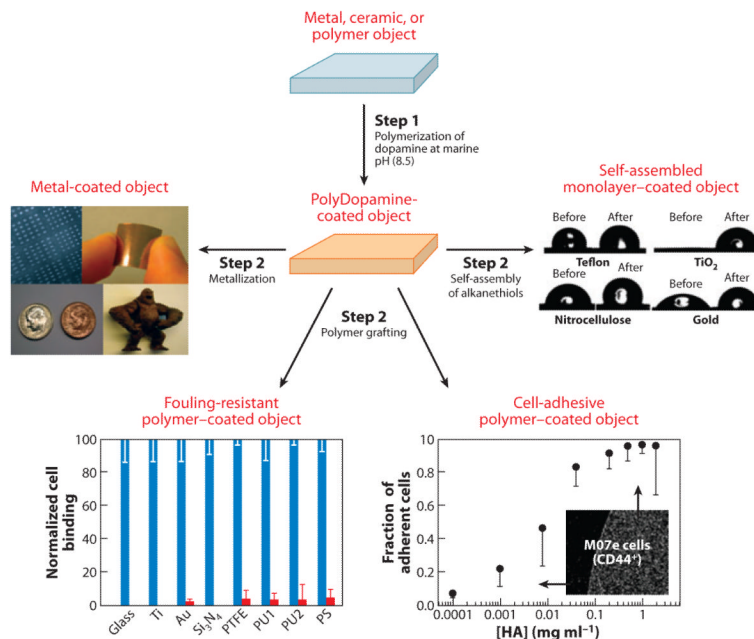


Figure 18. Mussel adhesive protein–inspired multifunctional coatings are derived from alkaline polymerization of a catecholamine such as Dopamine (101). Objects present in the solution become coated with a thin film of polyDopamine, which can be used as a base or primer for further functionalization of the surface with metal films, grafted polymers, or pseudo-self-assembled monolayers. Abbreviations: HA, hyaluronic acid; PS, polystyrene; PTFE, polytetrafluoroethylene; PU, polyurethane. Adapted from research originally published in Reference 38. Copyright © AAAS.

Table 1

Proteins of *Mytilus* byssus in or near the attachment plaque

Protein	Species	Mass (kDa)	pI	Dopa (mol%)	Sequence (consensus or complete) ^a	Repeat number	PTM ^b	Reference
Mfp-1	Me	108	10.5	15	[AKPSYO*OTYK] _n	75	O; O*	53
	Mc	90			[PKISO*OTYK] _n			47
Mfp-2	Mg	45	9.5	5	[TDKAYKPNPCVSKPKNRR GKCIWNGKAYRCKCAYGY GGRHC] _n	11	[S-S]	23, 22
	Me	6		20	ADYYGNYPGPRRYGGGNY NRYNRYGRRYGGYKGWNN GWNRRRGKYYW	1	R	26
Mfp-4	Mc	93		2	[HVHTHRVLHK] _n	36		28
					[DDHVNDIAQTA] _n	16		
Mfp-5	Me	9	9	28	SSEYKGGYYPGNAYHYSGG SYHSGSYHGGYKGYGK AKKYYKKNKNGKYLK ARKYHRKGYKYYGGSS	1	S	29
	Mc	11	9.5	3	GGNYRGCYCSNKGCRSGYIF YDNRGFCYKYGSSSYKYDCG NYACLPNYPGRVYCTKK YSCDDFYNNKGYYYND KDYGCFCGSYNGCCLRSY	1	S [S-S]	30
Tmp-1	Mg	57	9.5	3	[YGYGNYGYNGYNGKTNIIY NKSQYGYGNGYGYGNGYIYGY] _n	5		35
					[YGNKTTKIVVNGKNGYGYD] _n	3		
PreCOL-D	Me	240	10.5	<1	[GX ₁ X ₂] _n [A _n], n = 7-9	173	O	32
	Me	230	7.5	<1	[GX ₁ X ₂] _n	143	O	33

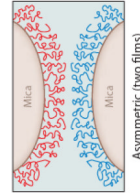
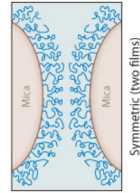
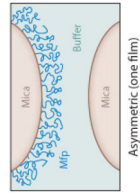
^aSymbols for standard amino acids follow convention.

^bPosttranslational modifications (PTM) are *trans*-4-hydroxyproline (O), *trans*-2,3-*cis*-3,4-dihydroxyproline (O), Dopa (Y), 4-hydroxyarginine (R), and *O*-phosphoserine (S). [S-S] denotes cross-linked Cys (C). A nonbolded C denotes any Cys whose oxidation state has yet to be determined. Species are *Mytilus edulis* (Me), *Mytilus galloprovincialis* (Mg), and *Mytilus californianus* (Mc). Other abbreviations: Mfp, mussel foot protein; PreCOL, prepolymerized collagen; Tmp, thread matrix protein. Dopa and *O*-phosphoserine also occur in other proteins besides those indicated, but their sequence position has not been determined.

Mussel foot protein (mfp) interaction strengths determined from thin films deposited on mica and tested in the surface forces apparatus. Conditions include a contact time of 60 min and buffer of 0.3-M KNO₃, 0.1-M acetate with pH 5.5 at room temperature^a

Table 2

Mfp	Dopa (mol%)	Adhesion work, asymmetric (mJ m ⁻²)	Hard wall (nm)	Adhesion work, symmetric (mJ m ⁻²)	Hard wall (nm)	Reference
<i>Intrinsic</i>						
Mefp-1	15	<0.1	8	<0.1	8	18
Mefp-2	5	<0.1	5	<0.1	10	24
Mefp-3 (pH 5.5)	20	0.3-0.5		0.3-0.5	10-40	29
Mefp-3 (pH 3)	20	1.2-1.4	4	1.2-1.4	5	29
Mefp-4	2	<0.1	13	<0.1	50	<i>b</i>
Mefp-5 (pH 5.5)	30	2.3-2.5	3			<i>b</i>
Mefp-5 (pH 3)	30	6-7	1-3			<i>b</i>
Mefp-6	3	<0.5	8	<0.5	12	31
Mefp-3 ↔ Mefp-5	20/30	2.3-2.6	3-8			<i>b</i>
Mefp-2 ↔ Mefp-5	5/30	1.2-1.5	12			24
<i>Metal mediated</i>						
Mefp-1 + Fe ³⁺ , <i>c</i>	15	0		4-5	8	56
Mefp-2 + Fe ³⁺ , <i>c</i>	5	0		2-3	12	24
Mefp-2 + Ca ²⁺ , <i>c</i>	5	0		0.2-0.4	15	24



^aMefp denotes *Mytilus californianus* foot protein; Mefp denotes *Mytilus edulis* foot protein.

^bUnpublished studies by J.H. Waite & J.N. Israelachvili

^cFe³⁺ and Ca²⁺ at 10 μM